The Multi-Purpose Bottom Plug for the Galataport Project

Salvatore Miranda, *Technical Manager, TREVI Turkey, Istanbul (Turkey); email: smiranda@trevispa.com*

ABSTRACT: *The paper describes an innovative geotechnical engineering solution that was provided by TREVI for the renovation project at Galataport in Istanbul, Turkey. Among other interesting geotechnical works included in the project, this paper also presents the design considerations and construction of the multi-purpose bottom plug (MPBP). This original geotechnical engineering solution was employed for a three-basement excavation in Karaköy and consists of a combination of seepage control, ground improvement, and load bearing elements, which were executed with double-fluid jet grouting, pseudo-elliptical jet grouting, and permanent micropiles, respectively. The paper describes each step of the design, execution, and the preliminary and final testing phases. Moreover, it highlights the importance of employing cutting-edge technologies used in deep foundation geo-construction and state-of-the-art electronic control devices, along with expertise, to obtain the desired results for this high-profile project.*

KEYWORDS: Ground improvement, Elliptical Jet Grouting, Bottom Plug, Liquefaction, Seepage Control, Micropiles.

SITE LOCATION: Geo-Database

INTRODUCTION

The Port of Galata (or Galataport) is a passenger terminal for cruise liners, situated in the Karaköy neighbourhood of the Beyoğlu district in Istanbul, Turkey. The port has up to 1,200 m of coastline and covers an area of approximately 100,000 m^2. It consists of two adjoining quays, the Karaköy (or Galata) Quay and the Salıpazarı Quay, extending from the Galata Bridge on the Golden Horn to Salıpazarı on the west coast of the Bosphorus. The construction of the Karaköy Quay began in 1892 and was completed in 1900. Two warehouses were built in 1910, and three more were added in 1928. The Salıpazarı Quay was built in 1957 by the Ministry of Public Works. The Port of Istanbul served as the country's biggest seaport for import cargo until 1986, when it became obsolete due to the increase of container shipping. In 1988, the port was converted into a passenger terminal for cruise liners and, in 2007, it was extended to meet the growing demand for cruise tourism.

Figure 1. Satellite view of the site before the renovation project's commencement.

The renovation project of Galataport began in 2014 and has involved the construction of a modern terminal for cruise ships, the construction of promenade along the coastline, and the restoration of historical buildings. The new terminal will play a pivotal role in the project since it is designed to be the first of its kind globally in underground boarding bridge systems for ships.

Submitted: 21 January 2019; Published: 21 May 2021
Reference: Miranda S. (2020). The Multi-Purpose Bottom Plug for the Galataport Project. International Journal of Geoengineering Case Histories, Volume 6, Issue 1, pp. 1-36, doi: 10.4417/IJGCH-06-01-01

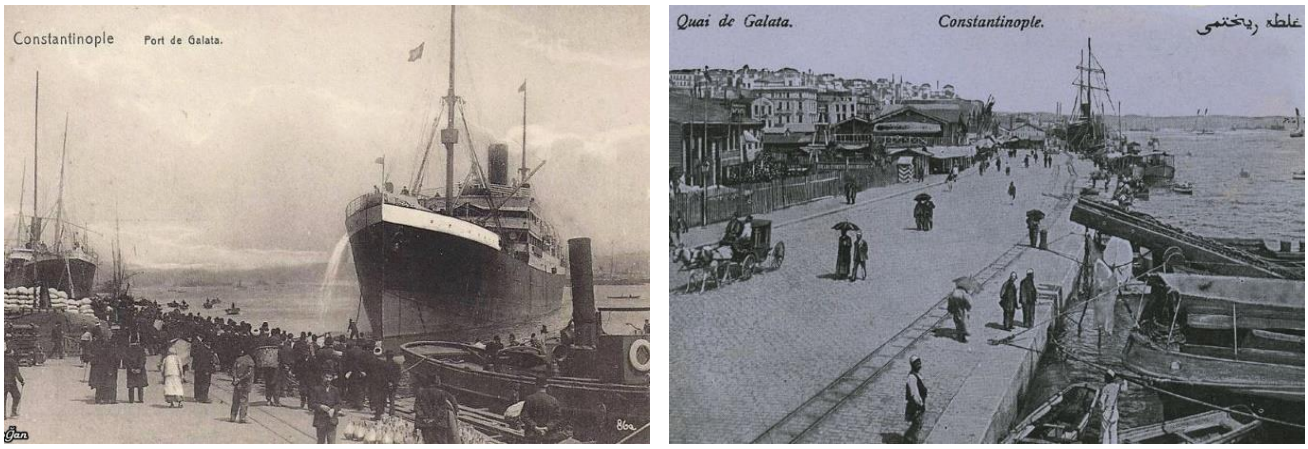

Figure 2. Early pictures of Karaköy (or Galata) Quay in the 1900s.

The contract for the geotechnical works was divided into two packages: Salıpazarı and Karaköy, which were first issued as two different tenders and were both eventually awarded to TREVI. The Salıpazarı package included mainly the construction of the new underground terminal. Prior to beginning the geotechnical works in this area, all existing old warehouses constructed in the late 1950s were demolished, except Antrepo 5 (*antrepo* means "warehouse" in Turkish), which is designated to be a museum of the Mimar Sinan University of Fine Arts. Antrepo 4 housed the Istanbul Modern, which was founded in 2004 as Turkey's first museum of modern and contemporary art. The new museum building is designed by Renzo Piano and is being reconstructed in its original site. The Karaköy package, instead, consisted of the refurbishment of an area that was fully occupied by five buildings. The historic structures were preserved and, after their strengthening and renovation, will be part of the new port facilities (Figure 3).

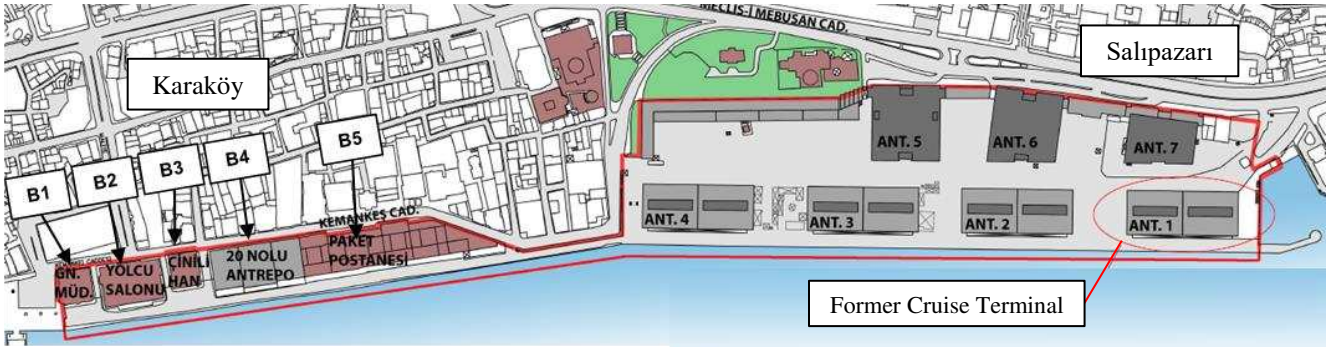

Figure 3. Schematic view of the original site condition, with highlighted existing buildings.

The difficult hydraulic and geotechnical conditions, the high seismic hazard of the site, the presence of historical buildings that needed to be restored and strengthened, the simultaneous execution of the new quay by other contractors, and the continuous operation of the port while construction activities were ongoing all required the employment of cutting-edge technologies within the foundation engineering field and caused additional difficulties to this high-profile project. Construction activities started in July 2016 and are ongoing at the time of the writing of this paper.

The tender concept design was deeply studied by the engineers of TREVI Design, Research, & Development Office, who proposed several technical improvements and alternative solutions, which resulted in a significant value engineering. Therefore, TREVI acted as both geotechnical contractor and proposal designer for the related works.

Among the interesting geotechnical works included in the Galataport project, this paper focuses on the design principles, adopted technologies, and performance controls related to an original geotechnical engineering solution adopted for the deep excavation of two buildings in the Karaköy site, one with two basements and the other with three.

THE KARAKŐY SITE

The Karaköy package, in addition to the re-construction of its portion of the quay, consists of the refurbishment of an area that was fully occupied by five buildings. Two historic buildings have been completely preserved, another two buildings have been partially demolished, and one non-historic building has been completely demolished.

This paper focuses on the design solution adopted for the deep excavation of the three-basement building that is being constructed in lieu of the demolished Bina 4 (*bina* means "building" in Turkish), which is also called Antrepo 20, and is highlighted by red rectangles in Figure 4. The solution was similarly applied also to Bina 2, which had two basement floors.

The foundation works within the footprint of demolished buildings Bina 2 and 4 consist of the following:

- A 1,000 mm thick propped diaphragm wall (D-wall) and secant pile wall executed by mechanical grab (18,000 m^2 of D-wall) and rotary piling rig (7,000 m of secant piles) along with 200 steel props,
- A hydraulic bottom plug to reduce groundwater flow during excavation and related settlements of adjacent buildings executed by 2,000 mm diameter double-fluid jet grouting overlapping columns (45,000 m^3 of treated soil),
- A lattice-type soil improvement against liquefaction composed of elliptical jet grouting columns (50,000 m^3 of treated soil), and
- A mesh of permanent tension micropiles against uplift, consisting of double corrosion protected (DCP) steel bars (10,000 m in total length).

As far as the preserved historical buildings are concerned, the related foundation works had to be conducted from inside the buildings with limited available headroom, and consisted of a massive soil improvement against liquefaction by means of 1,500 mm single-fluid jet grouting (40,000 m^3 of treated soil) and structural underpinning via micropiles to facilitate the excavation of a partial basement underneath.

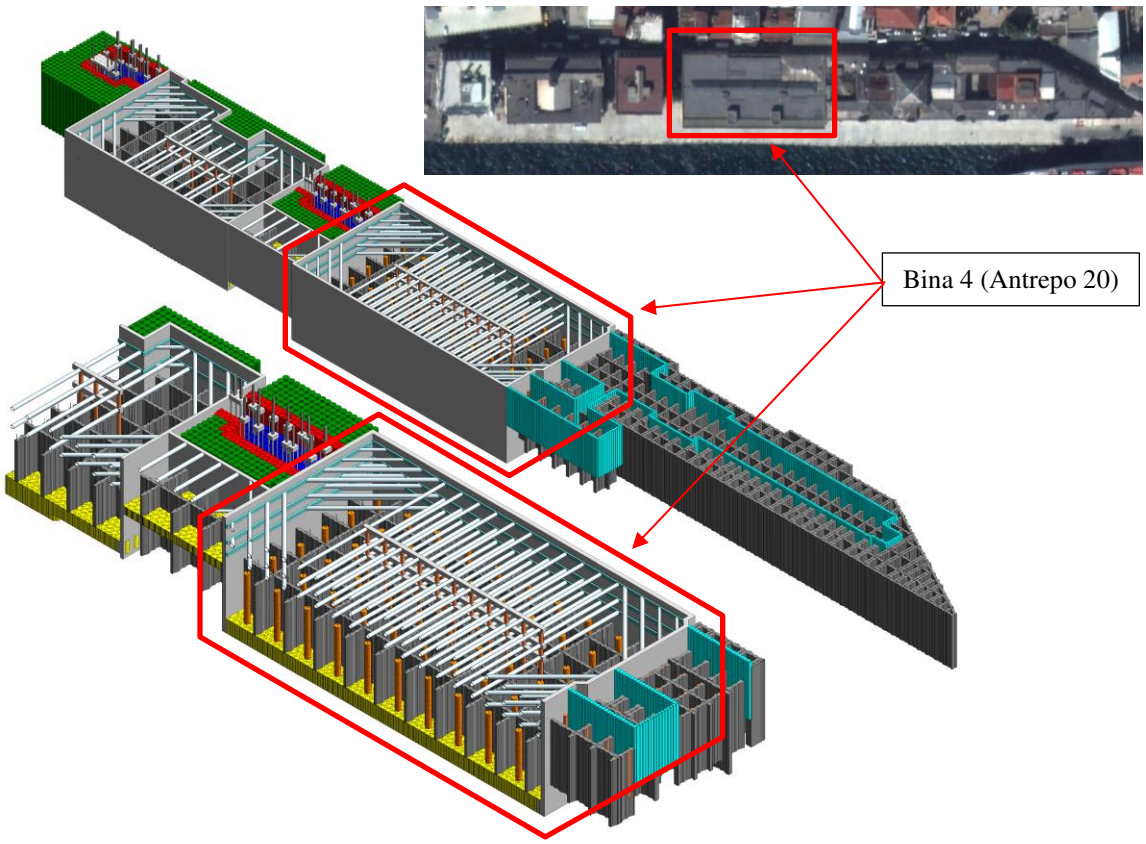

Figure 4. Schematic view of Karaköy site.

An extensive monitoring system was installed to control the behavior of the different components of the foundation system, the surrounding soil, and the existing buildings. All the aforementioned activities were executed almost simultaneously, which caused additional difficulties.

Soil Conditions at Bina 4

At the Karaköy site, the subsurface soil conditions are composed of a 25 m to 30 m thick layer of man-made fill (uncontrolled mixture of materials from clay to cobbles size) throughout the whole area. The fill is the result of the reclamation works executed in the last decades of the 1800s for the construction of the former Galata Quay. The ground surface is quite flat and its elevation ranges around El. +1.50 m msl, while the groundwater is at sea level (El. 0.00 m msl).

The thick fill layer is underlain by a layer of very loose silty sand that is about 5 m to 10 m thick. The bedrock is a very strong, very fractured Greywacke (UCS = 100 to 150 MPa), with the top 10 m to 15 m thickness being very weathered, as shown in Figure 7. The bedrock is located at a depth between 35 m and 45 m below the existing ground level, which is deeper than the geotechnical activities involved in this area; therefore, all structures were executed within the man-made fill and the underlying marine sand layer. The thick fill/sand layer contains a small amount of fine material and is classified as loose-to-very-loose (SPT N-values = 0 to 15 blow/0.3 m, qc = 0.5 to 3.0 MPa), with a high liquefaction risk. The permeability of this layer was assessed to be in the range of 10^{-4} m/s.

Figure 5. Loose-to-medium dense made ground (FILL).

Figure 6. Loose-to-medium dense silty SAND.

Figure 7. Very weathered GREYWACKE.

Challenges Related to the Deep Excavation of Bina 4

The three basement floors in Bina 4 have a rectangular footprint of about 45 m x 90 m in plan and a design excavation depth of 12.65 m, which is 11.25 m below sea level (Figures 8 and 9). The related excavation had to be conducted in a very confined area, which presented many associated risks. For example, on the two short sides of the excavation, there were two historical buildings: Bina 3 and Bina 5. The clear distance between the shoring system and the buildings was less than 0.5 m. On the landside of the excavation, Kemankeş Street is located only a few meters away from the shoring system and there are historical buildings that are 5 to 8 stories high on the opposite side of the road, at less than 15 m clear distance from the edge of excavation. Finally, at seaside, the shoring had to be executed at about 3 m clear distance from the existing quay, which was constructed in the 1900s and was constructed using rock blocks.

The main challenges related to the deep excavation of Bina 4 can be summarized as follows:

- Execution of shoring system in vicinity of the existing quay. The original idea of shoring included the execution of a 1000 m thick diaphragm wall, to be constructed with mechanical grab. The use of PVC waterstop bands to limit the risk of water leakage through the joints between the diaphragm wall panels was also foreseen. However, due to the reduced clear distance between the shoring and the existing quay, the bentonite mud could be easily and quickly lost from the excavated trench, through the rock blocks forming the existing quay. This fact, in addition to constituting an environmental problem, resulted in the collapse of one diaphragm wall panel and forced the engineers to opt for a change of technology, from the diaphragm wall to a fully cased secant pile wall. The solution was successful in terms of constructability but was worse in terms of the shoring weathertightness, which had to be expected and accepted.

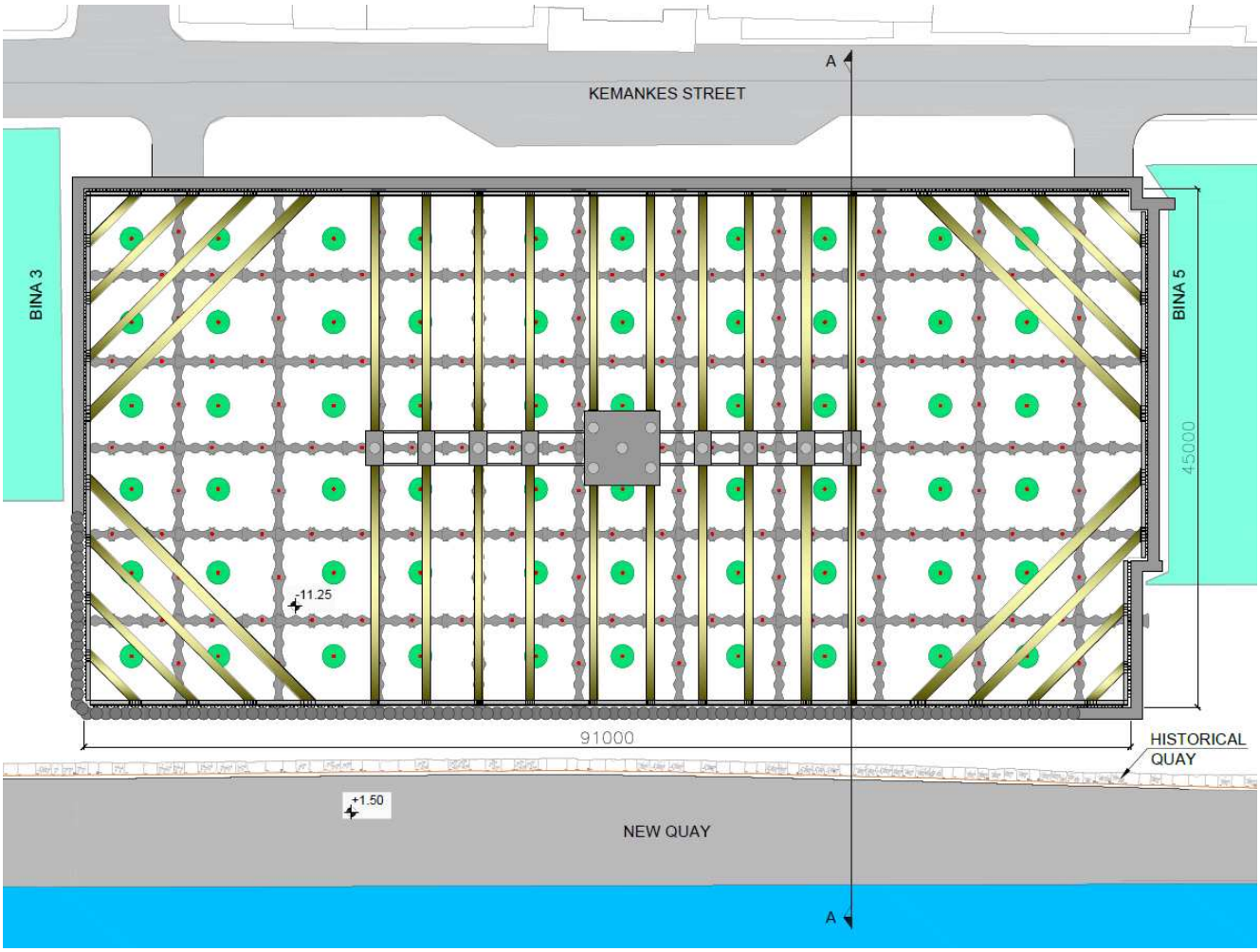

Figure 8. Plan view of Bina 4 geotechnical works.

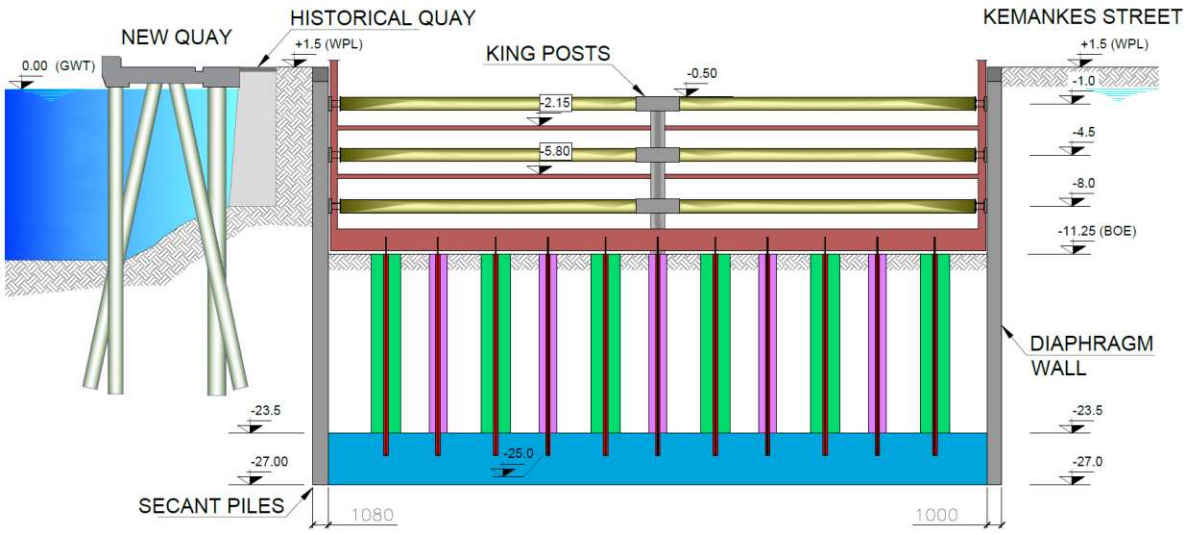

Figure 9. Section view of Bina 4 geotechnical works.

- Execution of shoring system in vicinity of the existing historical buildings. The construction of the diaphragm wall and the subsequent excavation of the pit in adjacency of the historical buildings Bina 3 and Bina 5 could have generated detrimental effects on the buildings. During the execution of the diaphragm wall, these could be mainly related to the vibrations, impact, and collapse of the open trench, while excessive settlements could be experienced during the basement excavation, associated with the lateral displacements of diaphragm wall. As preventive action, the massive jet grouting soil improvement works (100% of building footprint) from inside the nearby buildings was executed prior to beginning the execution of diaphragm wall. Moreover, a real-time monitoring system was set up on the building and measured the building settlements (both absolute and differential), vibration, and tilting of the façade. Some diaphragm wall panels were equipped with shape accelerometer arrays (SAA), while strain gauges were placed on the steel struts. The instrumentation provided a real-time response of the lateral displacements and strut forces generated by the diaphragm wall. Finally, temporary protection steel plates were mounted on the building historical façade to prevent damage related to the impact of the mechanical grab during trench excavation.

- Difficulties related to the lateral support of shoring. The site condition surrounding the shoring did not allow the installation of ground anchors. Therefore, a steel propping system, composed of 3 levels of 36 struts, was designed and constructed as lateral support of the shoring. This complicated the construction phases of the building with strut installation and removal phases and also complicated the logistics of the site due to the need of a tower crane and no free space for its installation. Horizontal struts were designed to span from the seaside to the roadside shoring, while inclined struts were designed for the four corners. Due to the significant length of the horizontal struts (about 45 m), it was decided to utilize intermediate king post piles to increase the buckling resistance of the strutting system. Moreover, king post piles were specially designed to be used also as the foundation of the tower crane so that one of the difficulties related to site logistics could be addressed (Figures 8 and 9).

- Seepage control. Due to the high permeability of the fill/sand layer (10^{-4} m/s) and to the significant hydraulic gradient, a total water flow of around 180 l/s was estimated for a conventional deep-well dewatering system. This could have been managed, barely, by a proper number of submergible pumps. Moreover, it was also assessed that the lowering of the water table associated with the deep-well system could have produced undesired settlements of the nearby historical buildings. Therefore, it was decided to not take the risk and to go for a bottom plug, which would have reduced the equivalent permeability of the system and consequently limited the total water seepage.

- Liquefaction risk. Istanbul is characterized by high seismicity and the very loose and saturated fill/sand layer was deemed to be susceptible to liquefaction under the design earthquake of Moment Magnitude Mw 7.0 and peak ground acceleration of 0.3 g. Initially, a soil improvement program using vibro-flotation was considered; however, additional investigation and analysis highlighted the risk of damage to the nearby historical buildings that may have been caused by the vibrations of this technology. Therefore, a lattice-type soil improvement was proposed by TREVI as remediation to liquefaction.

- Uplift of the building. The designed Bina 4 is a low-rising building and its weight is not sufficient to counteract the 120 kPa of uplift water pressure acting at its base. In the temporary condition with only three basement floors constructed, the uplift water pressure would be greater than the bearing pressure at the bottom of the slab. In the permanent condition, the bearing pressure would be greater than the uplift water pressure in some areas of the foundation where concentrated loads would be acting. To resist the uplift force during and after the building construction, a regular mesh of 1000 mm diameter tension piles was foreseen. However, it was proposed by TREVI to substitute those bored piles with a system of permanent micropiles with a diameter of 250 mm composed of DCP steel bars. Even though the micropiles provide a much lower lateral surface per unit length compared to the bored piles, the idea was to combine them with the lattice type soil improvement to rely on a higher unit shaft friction compared to that associated with the loose fill/layer.

The multi-purpose bottom plug was designed and executed by TREVI to simultaneously address seepage control, liquefaction risk, and uplift of the building.

THE MULTI-PURPOSE BOTTOM PLUG

The multi-purpose bottom plug (MPBP) is an innovative geotechnical solution, which is formed by a combination of seepage control, ground improvement, and load bearing elements (Figures 10 and 12).

The main body of the bottom plug is composed of overlapping jet grouted circular columns executed with the double-fluid method and designed to have a diameter of 2,000 mm. The columns are executed on a triangular pattern with an average center-to-center spacing of 1,450 mm. The thickness of the bottom plug is the one constraint necessary to ensure the hydraulic stability of the excavation.

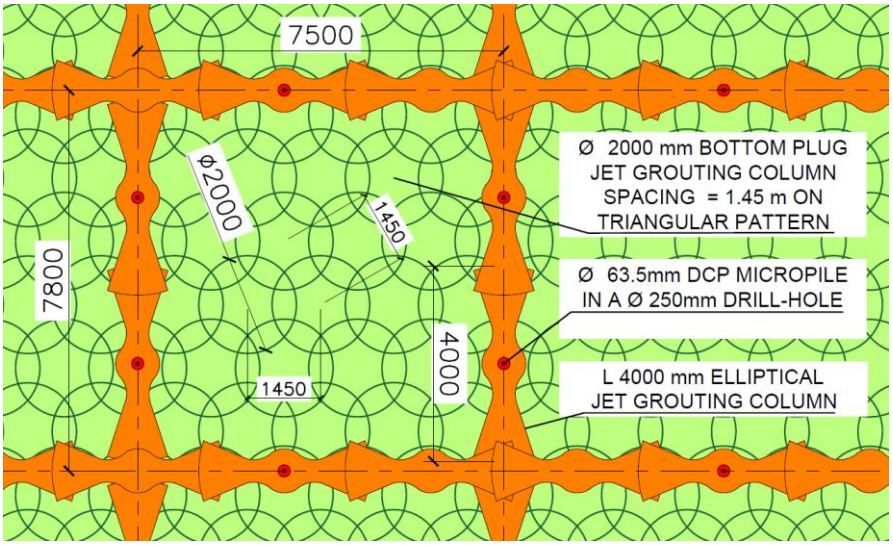

Figure 10. Details of single MPBP element – Plan view.

The pseudo-elliptical jet grout columns are executed from the top of the bottom plug up to the excavation level on a lattice-type pattern to act as a mitigation element against liquefaction. The pseudo-elliptical shape of the jet grout columns was chosen instead of a circular shape to optimize the lattice geometry, by minimizing the amount of jetting and the related time of execution. The lattice-type jet grouting treatment also acts as a foundation for the future building and will carry the vertical structural loads in the permanent condition in the areas with localized compression loads at the foundation. The average length of the elliptical jet grout columns, in the plan view, is 4.0 m.

The lattice-type soil improvement was executed using the pseudo-elliptical jet grouting (EJG) technology. This system was patented by TREVI and creates such a column shape by modifying the rotation speed in a planned way. The rotation speed varies from Vr1 to Vr2 to create the variable radius sectors (Figure 11).

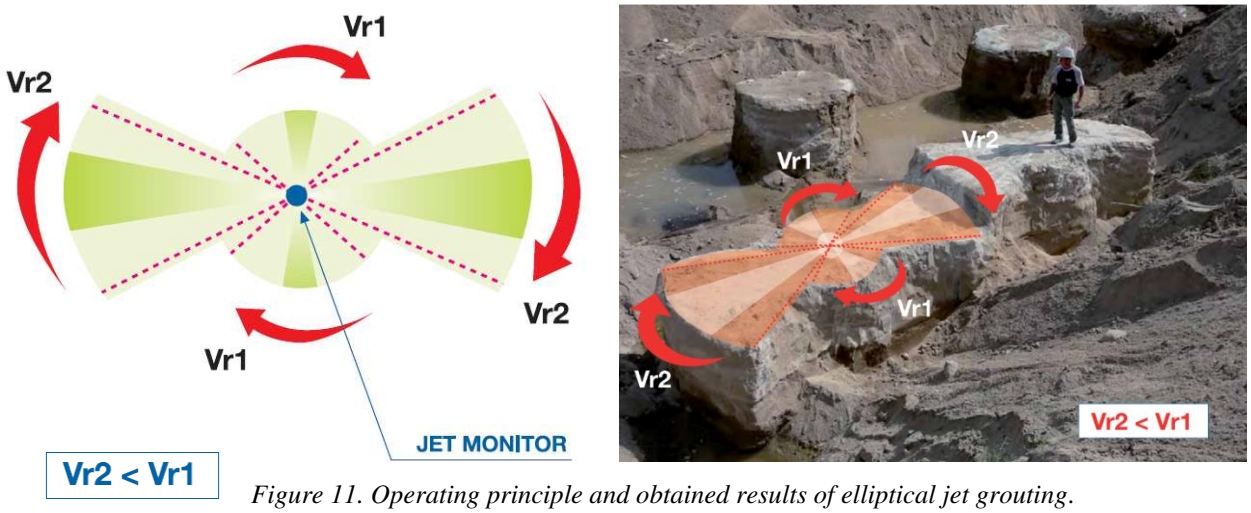

Figure 11. Operating principle and obtained results of elliptical jet grouting.

The stability against uplift is ensured by the permanent DCP steel bars, which are installed as drilled-and-grouted micropiles through the previously-executed elliptical jet grout columns. The DCP steel bars have a diameter of 63.5 mm and are installed within a 250 mm diameter drill hole. The system is designed with the uplift force acting in the temporary condition (only the three basement floors constructed), which represents the worst scenario.

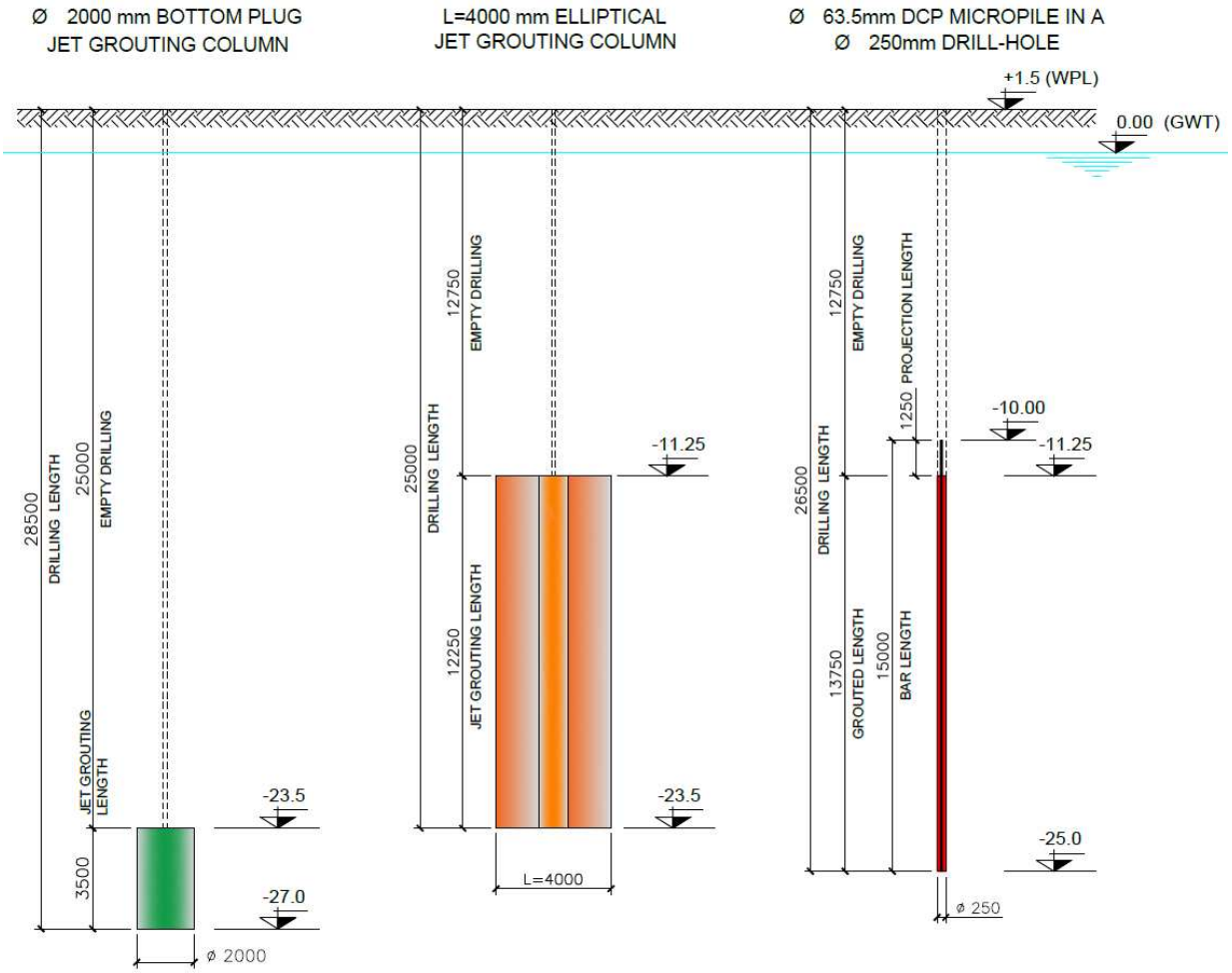

Figure 12. Details of single MPBP element – Vertical section.

DESIGN PRINCIPLES

The design of the MPBP was executed by TREVI, in collaboration with ENAR, the client's geotechnical consultant, and ITASCA.

Seepage Control

The main characteristics of the jet grout bottom plug were designed based on following principles:

- Depth. A verification for uplift (UPL) was carried out according to Eurocode 1997-1 by checking that the design value of the combination of destabilizing permanent and variable vertical actions (*uplift water pressure acting underneath the plug*) was less than or equal to the sum of the design value of the stabilizing permanent vertical actions (*sum of weights of jet grouting plug and that of the overburden soil*).
- Thickness. The minimum thickness of bottom plug was defined by limiting the hydraulic gradient to a value near 3, which was considered acceptable. Given the difference in piezometric height of $\Delta H = 11.25$ m, a hydraulic gradient of $i = 3.2$ was obtained with a bottom plug thickness $H = 3.5$ m.
- Permeability. Based on literature and previous TREVI experience, the permeability of the in-situ soil can be reduced by two or three orders of magnitude when jet grouting is executed.
- Strength. No minimum strength requirements were specified since the bottom plug was non-structural.
- Column spacing. All jet grouting columns were executed on a triangular pattern established on the existing working platform at an elevation of El. +1.5 m msl. Their center-to-center spacing was designed to ensure a sufficient overlap among all adjacent columns, after considering a certain vertical deviation of each column. A probabilistic analysis was run, in which the vertical deviation of the column was considered to vary randomly among a Gaussian distribution of values. Such distribution was based on previous and similar TREVI experiences and had a median value of vertical deviation equal to 1.0%. A center-to-center column spacing of 1.45 m was selected.

Liquefaction Risk Mitigation

Lattice-shaped ground improvement using soil-cement mixtures has often been developed as a solution against soil liquefaction. The idea is to create a grid of improved soil to retain the untreated soil in between and to control its shear deformation during an earthquake, preventing the rising of excess pore water pressure and possible liquefaction.

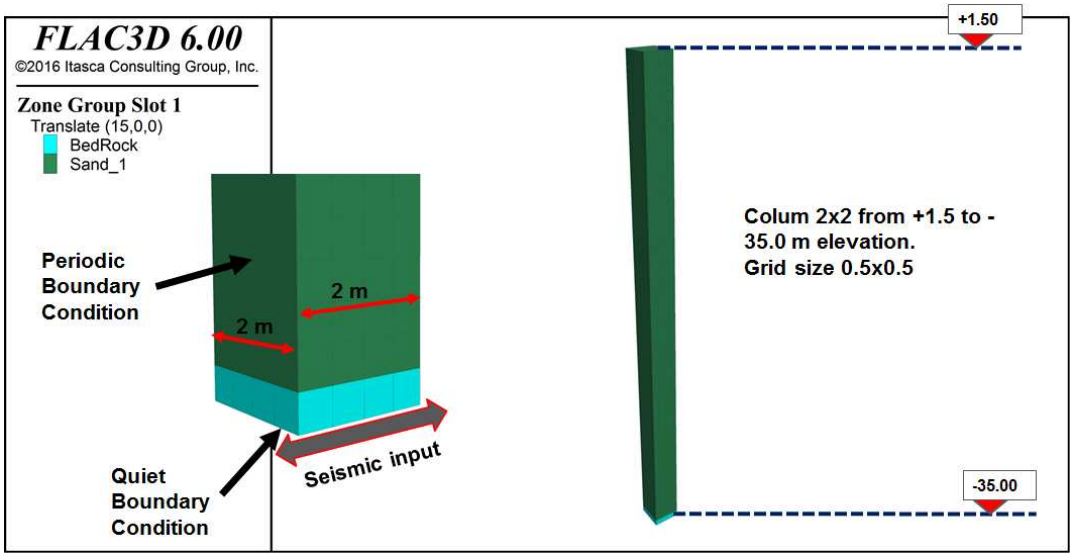

Figure 13. FDM model of natural soil for non-linear time history analysis.

The satisfactory performance of this method was confirmed following the 1995 Hyogo-ken Nanbu (Kobe) earthquake, and applications using such a design concept have increased since. There are several studies on the efficacy of lattice-type soil

improvement as a mitigation to liquefaction, including laboratory tests (e.g., shaking table tests and centrifuge experiments) and numerical analyses (e.g., dynamic 3D FEM/FDM analyses). References can be found in Namikawa et al (2007) and Takahashi et al (2006, 2013).

To design the MPBP unit cell, a non-linear time history 3D FDM analysis was carried out using FLAC3D. The liquefaction potential of the natural soil was analyzed on a 35 m deep, 2 m x 2 m sand column bordered by periodic boundaries (Figure 13). The seismic input was applied at a bedrock elevation of El. -35.0 m msl (quite boundary). Regarding the assessment of the mitigation effect on the treated soil, three different cell net sizes were considered: 5 m x 5 m, 7 m x 7 m, and 10 m x 10 m. The main details of the models are shown in Figure 14. The strength and deformation properties of the soil improved by the jet grouting were defined as UCS = 5 MPa and Es = 5 GPa.

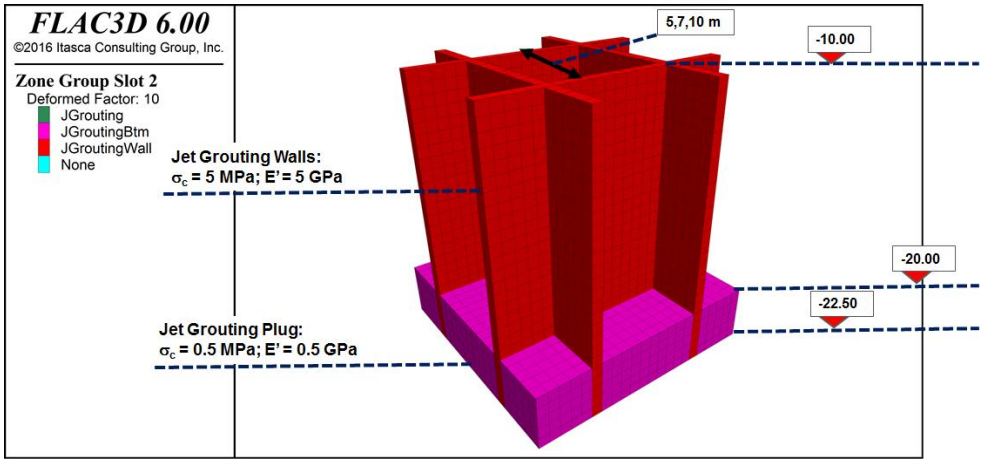

Figure 14. FDM model of lattice-type jet grouting cell for non-linear time history analysis.

The seismic input considered for the analysis was the Izmit-Kocaeli event of 17 August, 1999 (Figure 15). This event was located relatively close to the site and has been recorded on an outcrop, meaning that there is no need for deconvolution. It can be directly applied to the base of the model (bedrock position). The velocity history has been transformed to a shear stress history applied at the base of the model using the following:

$\sigma_s = -2 \cdot \rho \cdot C_s \cdot V_{seis}$

where:

- σ_s = stress at bedrock;
- ρ = density of the bedrock;
- C_s = shear wave velocity at the bedrock; and
- V_{seis} = incoming seismic velocity history at the bedrock.

The factor 2 accounts for the quiet boundary condition which absorbs half of the seismic input. In this case, since the outcrop motions include the free surface effect which amplify the seismic signal by a factor of 2, the input stress history becomes:

$\sigma_s = \cdot \rho \cdot C_s \cdot V_{outcrop}$

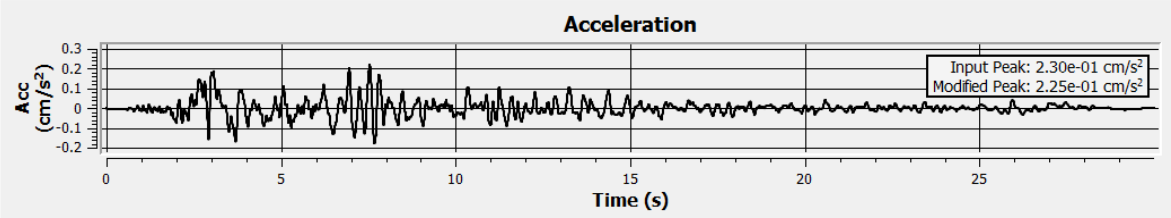

Figure 15. Izmit-Kocaeli time histories (Source: PEER NGA strong motion database record).

The results of the main analysis are shown in Figures 16 and 17: the red points are those where the ratio R_u between the excess pore pressure and the effective vertical stress reach the value of 1. It is possible to notice that, in natural soil, liquefaction occurs down to a depth of 24 m below the groundwater table. Instead, in the presence of the soil improvement, the value of R_u approaches 1 in just a thin band beneath the soil treatment. The 7 m x 7 m grid was selected; the 10 m x 10 m option provided satisfactory results but presented some local liquefaction phenomena at the surface of the excavation.

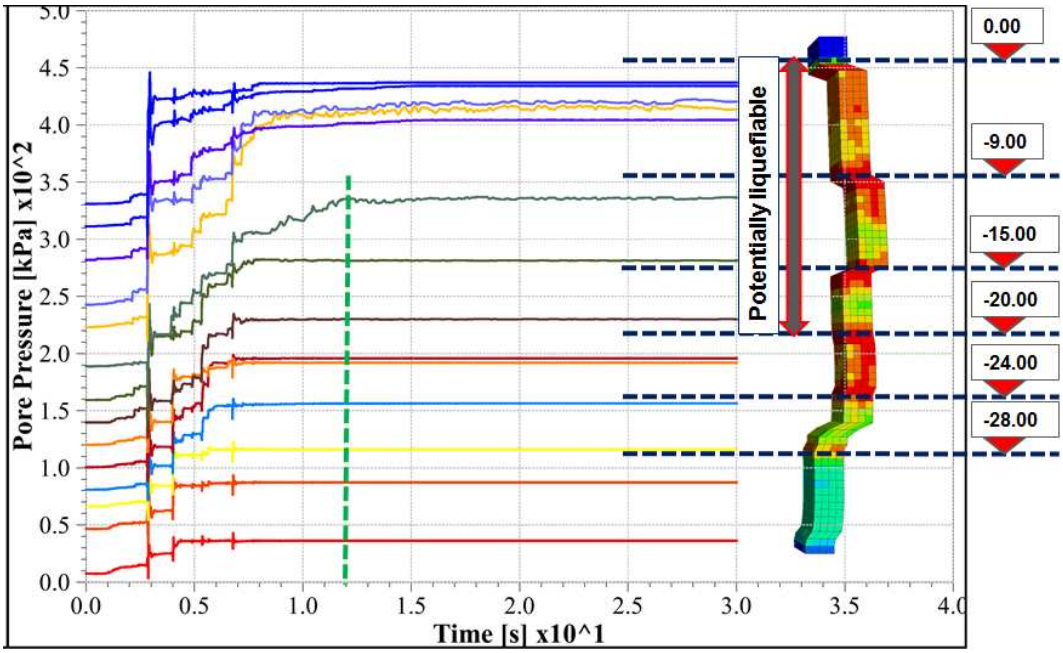

Figure 16. Pore pressure history and Max Ru in natural soil.

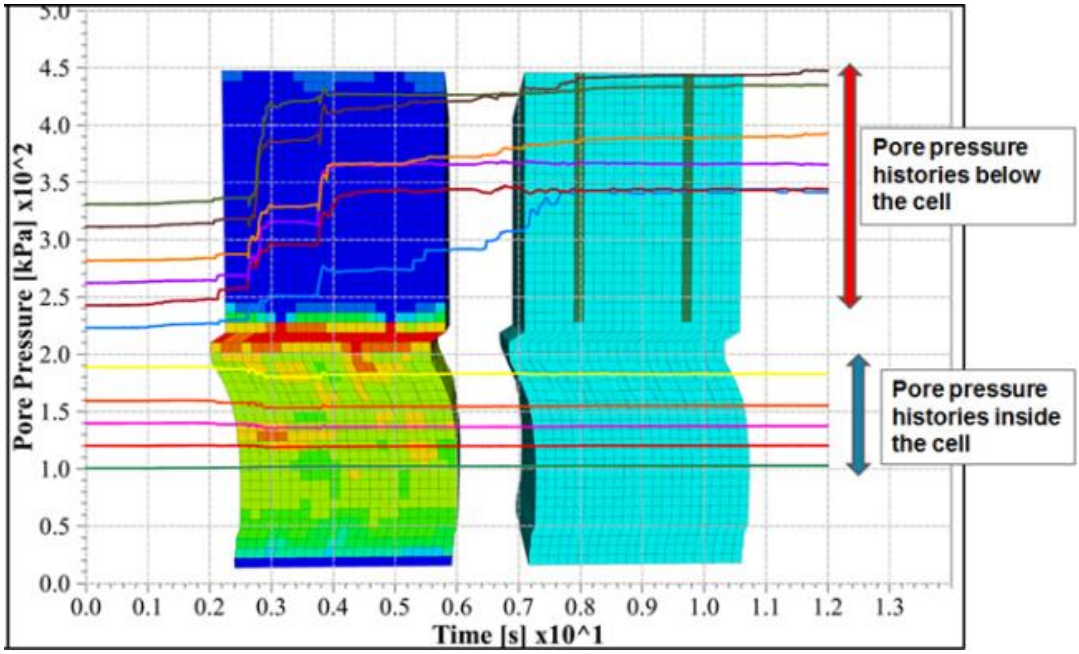

Figure 17. Pore pressure history and Max Ru in improved soil.

The different coloured lines in Figures 16 and 17 represent the pore pressure history at various depths. The two green rectangular blocks in Figure 17 represent the cross section of the jet grouting cell.

The maximum recorded shear stress in lattice-type jet grouting is shown in Figure 18 below and is expressed in kPa.

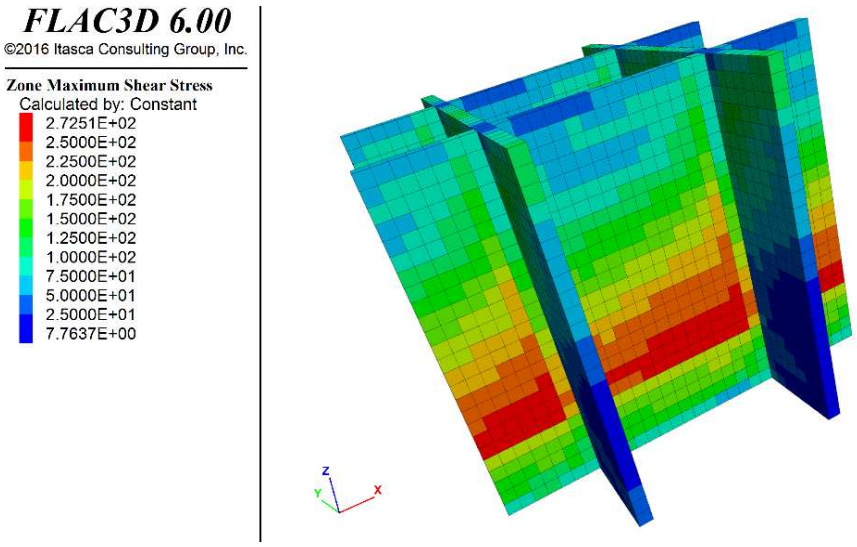

Figure 18. Maximum recorded shear stress in jet grouting cell, expressed in kPa.

Stability Against Uplift

To resist the uplift water pressure acting beneath the building during and after its construction, a system of DCP steel bars was designed (Figure 19). Once the jet grout column had reached an adequate value of unconfined compressive strength, the permanent micropiles were installed within a 250 mm drill hole and were installed through the elliptical jet grout column (Figure 20). In this way, the greater cross section of elliptical jet grouting column was used for facilitating the transfer of tensile force from the steel bar to the in-situ soil. Only in Bina 4 where the total uplift force was significant, extra 2,000 mm jet grout columns were installed in between the lattice-type grid, with the only scope of allowing the installation of the necessary number of permanent micropiles. Such circular jet grouting columns were shown in green in Figures 8 and 9.

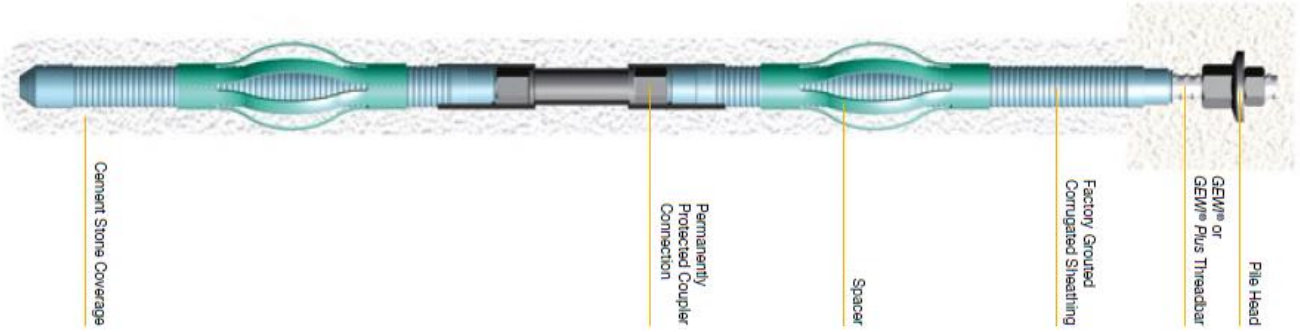

Figure 19. Details of proposed DCP rebar.

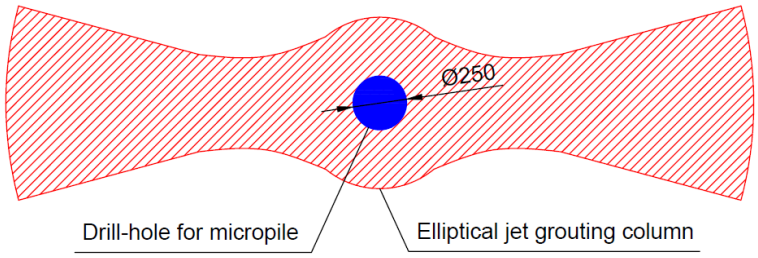

Figure 20. Scheme of rebar installation within elliptical jet grouting column.

The whole system of permanent micropiles was designed in order to avoid the following types of failure:

1. Structural resistance of steel rebar
2. Bar-to-internal grout failure
3. Corrugated PVC-to-external grout failure
4. External grout-to-jet grouting column failure
5. Internal failure of jet grouting column and respect to surrounding soil
6. Global uplift failure of whole system

The average working load per micropile in the temporary condition (worst case scenario) was calculated as 1,385 kN. While most of the above listed verifications are straightforward, failure modes 4 and 5 deserve a small discussion regarding the assumptions made for the verification.

Failure Mode 4 - External Grout-to-Jet Grouting Column Failure:

The maximum average shaft friction $\tau_{k,1}$ acting along the 250 mm diameter micropile shaft can be calculated as:

$$\tau_{k,1} = \frac{N_k}{\pi \times \phi_d \times L_b} = \frac{1385\ kN}{\pi \times 0.25\ m \times 13.75\ m} \cong 128\ kPa \quad (1)$$

where:

N_k characteristic tensile load on single micropile;

ϕ_d micropile drilling diameter; and

L_b micropile bond length.

The nominal grout-to-ground bond strength is evaluated through the Horvath and Kenney formula:

$$f_s = 0.65\, p_a \sqrt{\left({}^{q_u}/_{p_a}\right)} \quad (2)$$

where:

p_a atmospheric pressure (0.1 MPa); and

q_u uniaxial compressive strength of jet grouting (5 MPa).

From which the ultimate unit shaft friction can be calculated as:

$$f_s = 0.65 \times 0.1\ MPa \sqrt{\left({}^{5\ MPa}/_{0.1\ MPa}\right)} \cong 460\ kPa \quad (3)$$

Thus, the safety factor available at micropile shaft surface is:

$$SF_1 = \frac{460\ kPa}{128\ kPa} = 3.59 \quad (4)$$

Failure Mode 4 - Internal Failure of Jet Grouting Column and Respect to Surrounding Soil:

This check is executed to ensure that the jet grout column will not fail internally or externally under the applied tensile load. First, it is ensured that the jet grout column can resist the applied shear stresses at its minimum cross section (highlighted in green in Figure 21).

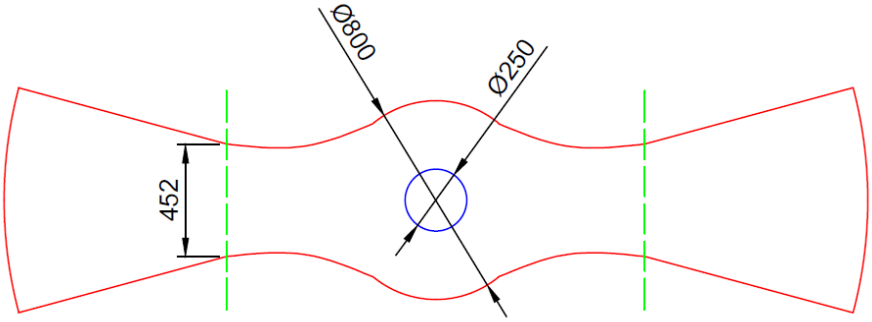

Figure 21. Typical scheme of micropile through the elliptical jet grouting column.

The maximum average skin friction acting along the minimum cross section of the jet grout column can be calculated by disregarding the grout-to-ground skin friction resistance on the two long sides of the column, for safety reasons:

$$\tau_{k,2} = \frac{N_k}{2 \times t_{min} \times L_b} = \frac{1385\ kN}{2 \times 0.45\ m \times 13.75\ m} \cong 112\ kPa \quad (5)$$

Where:

N_k characteristic tensile load on single micropile;

t_{min} minimum cross section thickness of jet grouting column; and

L_b micropile bond length.

The maximum allowable shear stress within the jet grout column can be calculated according to chapter 12 (plain concrete) of EC2:

$$\tau_{c0} = \frac{f_{ctd}}{K} = \frac{\alpha_{ct}}{1.5} \times \frac{0.7 \times \left(0.3 \times f_{ck}^{2/3}\right)}{\gamma_c} = \frac{0.8}{1.5} \times \frac{0.7 \times \left(0.3 \times 5^{2/3}\right)}{1.5} = 218\ kPa \quad (6)$$

Therefore, the safety factor available against jet grouting failure is:

$$SF_2 = \frac{218\ kPa}{112\ kPa} = 1.95 \quad (7)$$

Once it was verified that the jet grouting column would not fail under the applied shear stress, it was checked that the tensile force could be transferred from the steel bar to the surrounding soil through the shaft friction, between the elliptical jet grout column and the soil itself. For simplicity's sake, the jet grouting column was considered as a rectangular barrette with dimensions of 1 m x 4 m.

PRELIMINARY FIELD TESTS

Comprehensive preliminary field tests were executed to verify each of the design assumptions and to define the best operational parameters. The trial field tests were conducted within the Bina 4 footprint to evaluate in the same conditions that would have been found during installation of working elements.

Seepage Control & Liquefaction Risk Mitigation (Double Fluid and Elliptical Jet Grouting)

For the double-fluid jet grouting for the bottom plug and the elliptical jet grouting for the lattice-type soil improvement, two isolated jet grouting columns (B-JG-1 and B-JG-2 for the bottom plug, and E-JG-1 and E-JG-2 for the elliptical jet grouting) with different operational parameters were installed. One continuous coring and one seismic crosshole tomography line were executed for each column to assess the column diameter/length in plan and the overall quality of the jet grouting.

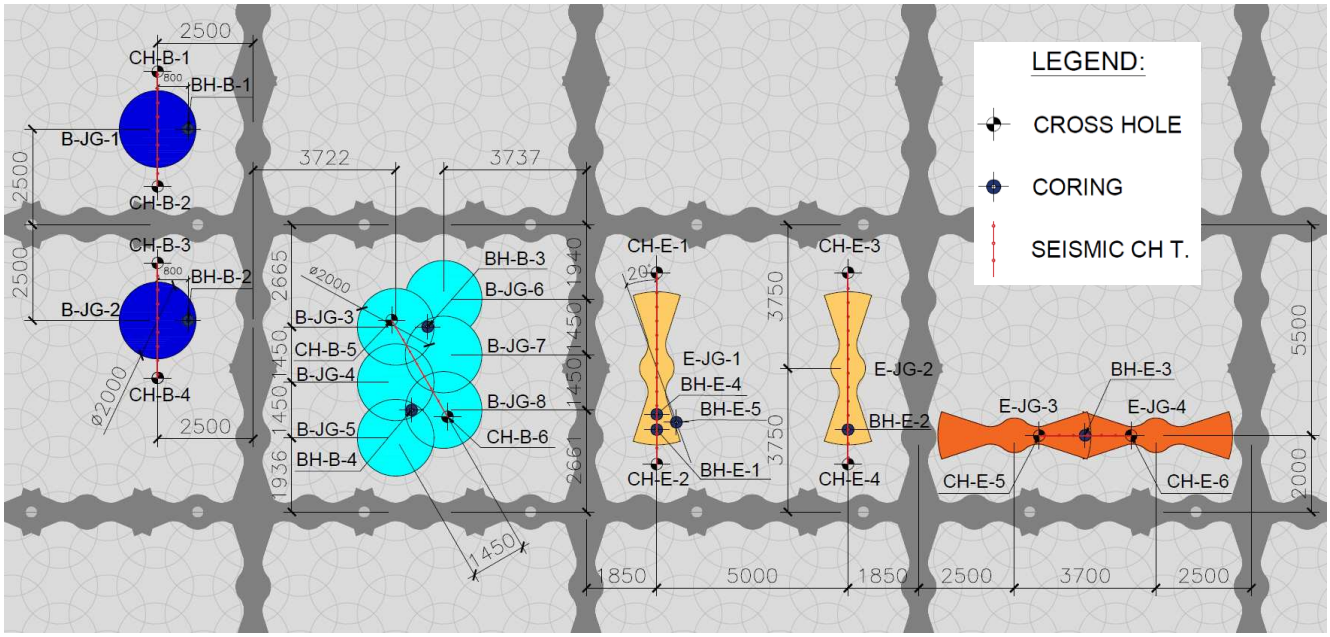

Figure 22. Plan view of the jet grouting preliminary field test.

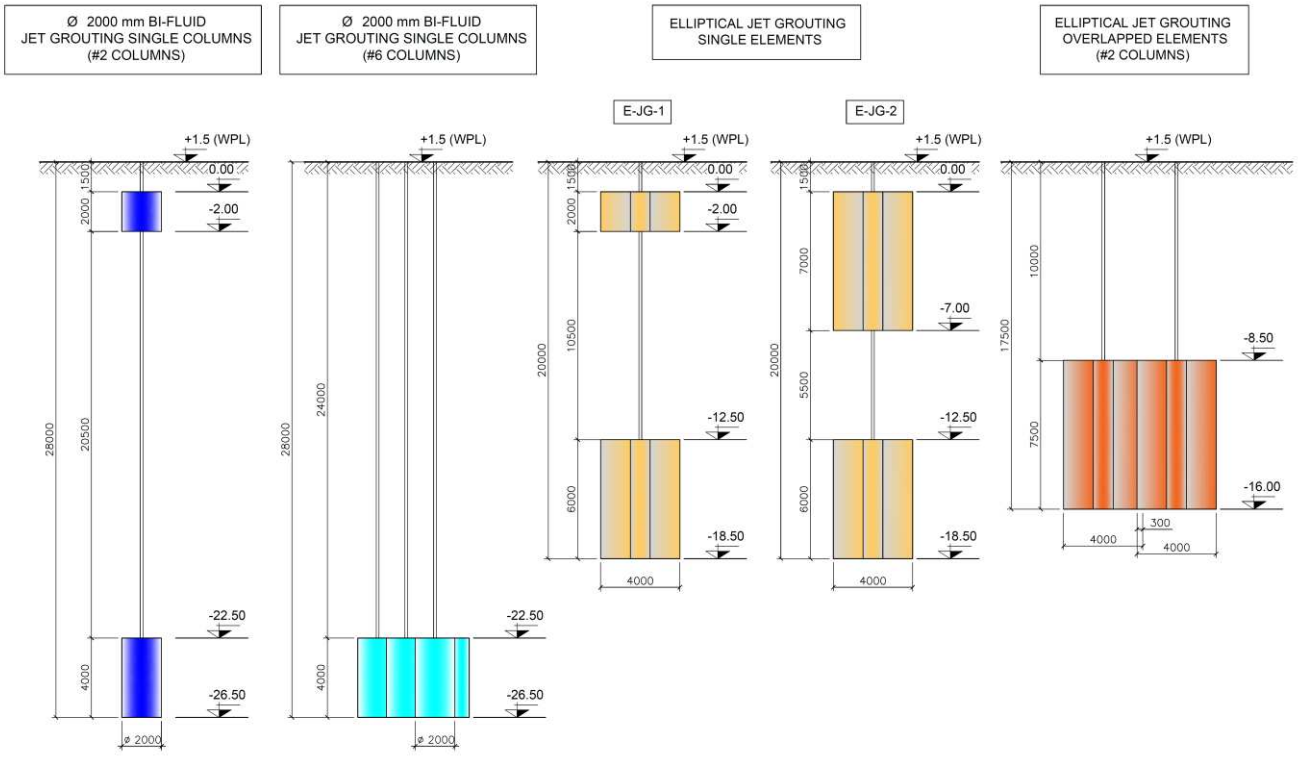

Figure 23. Section view of the jet grouting preliminary field test.

General details of the preliminary field tests can be found in Figures 22 and 23. Based on the results of the seismic crosshole tomography for the double fluid jet grouting for the bottom plug, both of the single columns fulfilled the design diameter; however, the B-JG-2 column showed a slightly bigger and better defined diameter as well as more satisfactory results of homogeneity of the treatment (Figure 24). Therefore, the operational parameters of column B-JG-2 were used to install a

group of six overlapping columns (B-JG-3 to 8) at the design depth of bottom plug. Two continuous corings were executed in the overlapping zones and one seismic crosshole tomography line was also conducted across the columns to verify the presence and quality of the overlapping. Pictures of one coring (BH-B-3) and measured values of shear wave velocity (Vs) can be found in Figure 25. The results of the seismic crosshole tomography executed on the overlapping columns show a full overlapping and continuity in the block of treated soil without relevant defects. The median measured value of Vs was 640 m/s.

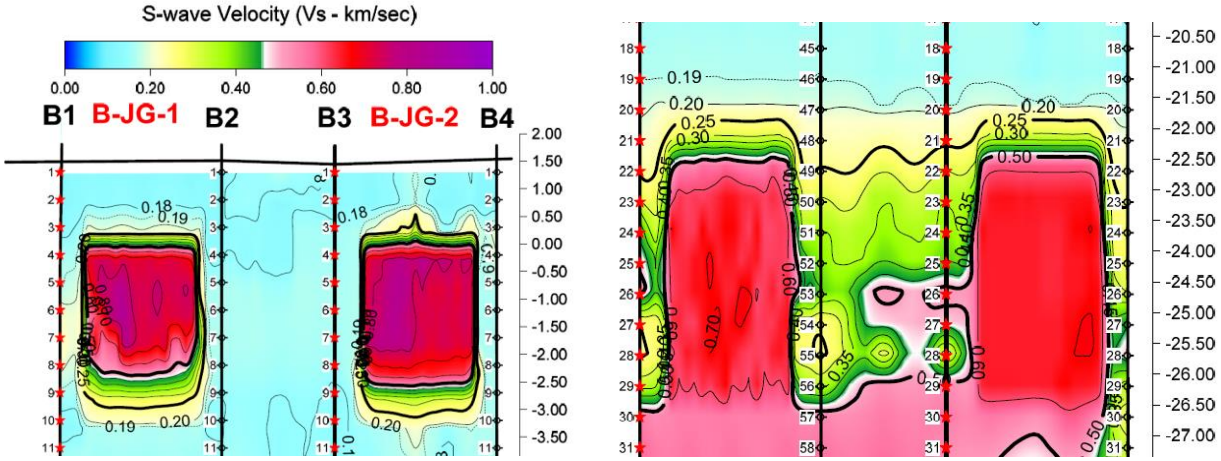

Figure 24. Measured Vs for columns B-JG-1 and B-JG-2 at two different depths.

Regarding the elliptical jet grouting, it was necessary to verify that the design column length of 4 m could be obtained (i.e., column E-JG-2 in plan Figure 22). This was an ambitious goal since it had been rarely achieved in previous attempts. Based on the seismic crosshole tomography, an anomaly emerged for column E-JG-1 since its length in plan resulted to be around 1 m. For column E-JG-2, instead, a column width in plan greater than 4 m was assessed (Figure 26). This was not in agreement with the utilized operation parameters and, after further investigation, it was found that the column E-JG-1 had been executed with a rotation in plan of about 20° (Figure 22). This was defined by means of specifically executing coring BH-E-1, 4, and 5.

Figure 25. Core box photos of coring BH-B-3 between 24 and 29 m depth. Measured Vs across overlapping columns.

Several cracks were visible on the extracted core, which could be due to the coring effects but could be also related to the overlapping of two different jet grouting columns.

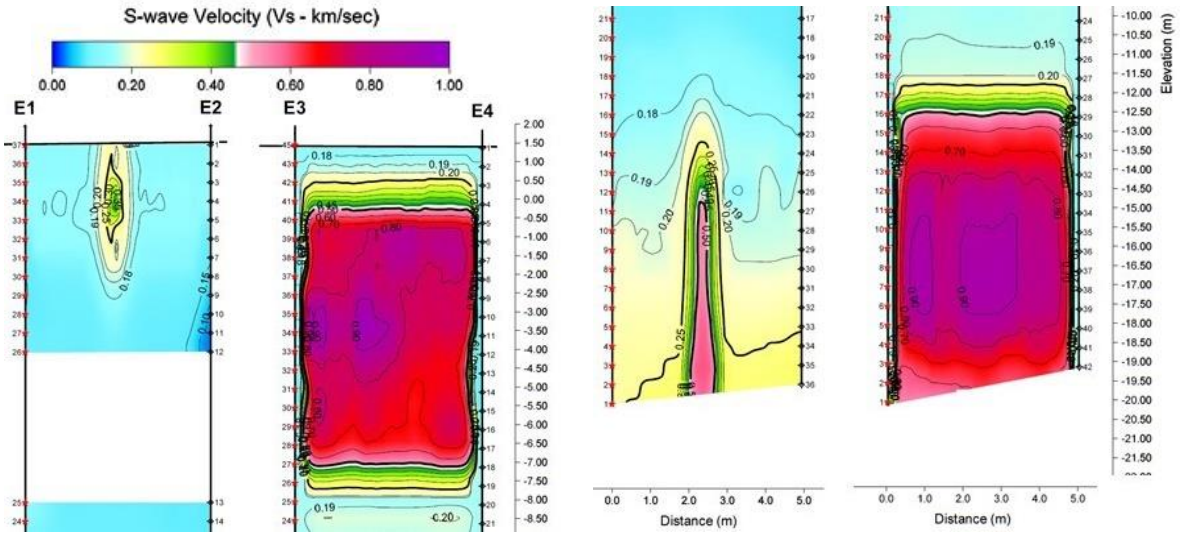

Figure 26. Measured Vs for E-JG-1 and E-JG-2.

The operational parameters of column E-JG-2 were used to install a set of two overlapping columns (E-JG-4 and 5). One continuous coring was executed through the overlapping and one seismic crosshole tomography line was also conducted across the columns to verify the presence and quality of the overlapping. Pictures of the core boxes and the measured values of shear wave velocity (Vs) can be found in Figure 27. Several cracks could be seen on the extracted core, which could be due to the coring effects but could be also related to the overlapping of two different jet grouting columns. Moreover, it should also be considered that these jet grouting columns were executed within the man-made fill, which included bricks and blocks.

The results of the seismic crosshole tomography executed on the overlapping columns show a full overlapping and continuity between the two columns without relevant defects. The median measured value of Vs is 920 m/s.

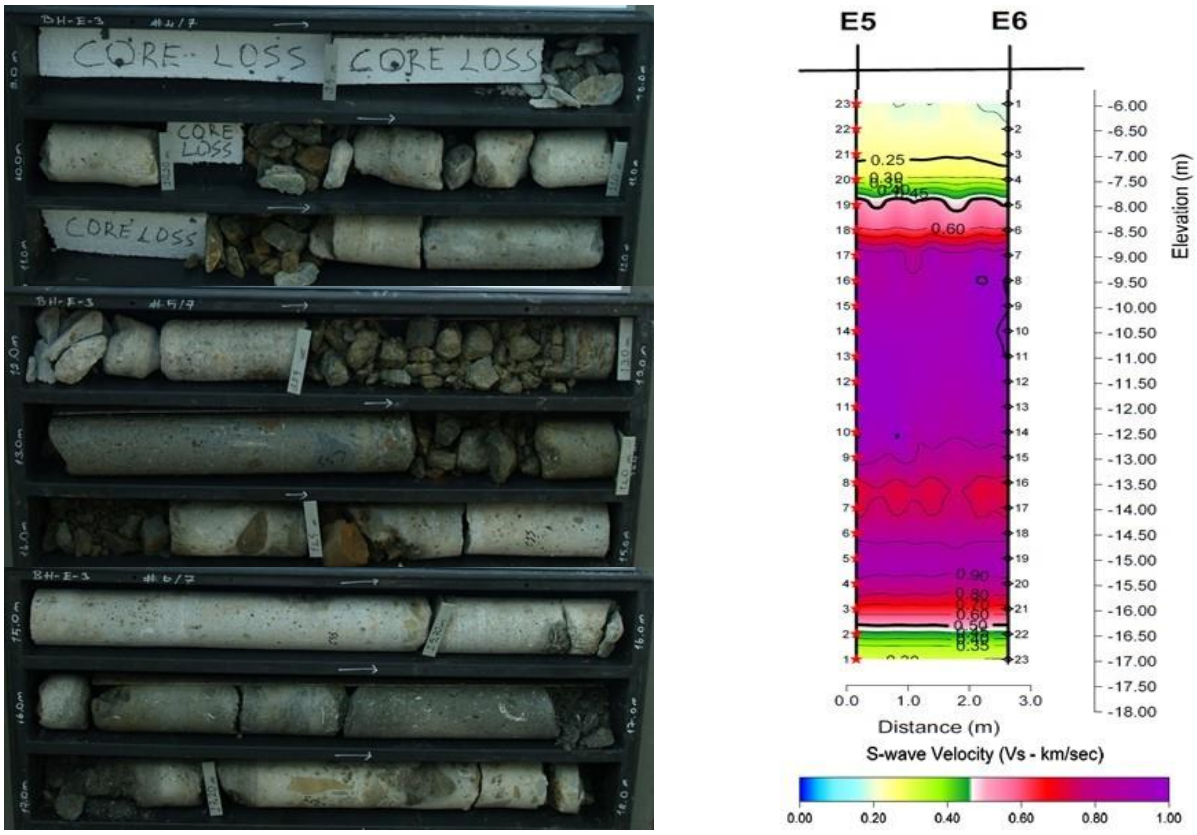

Figure 27. Core box photos of coring BH-E-3 between 9 and 18 m depth. Measured Vs across overlapping columns.

The elliptical jet grouting forming the MPBP was designed to create a stiff grid that would prevent the loose sand from liquefying in the event of earthquakes. For this reason, it was specified that the soil improved by jet grouting should have an average unconfined compression strength (UCS) greater than 5 MPa and an average elastic modulus (Es) greater than 5 GPa. This was verified by laboratory tests on core samples taken from the preliminary field trial test columns. The results were satisfactory (Figure 28).

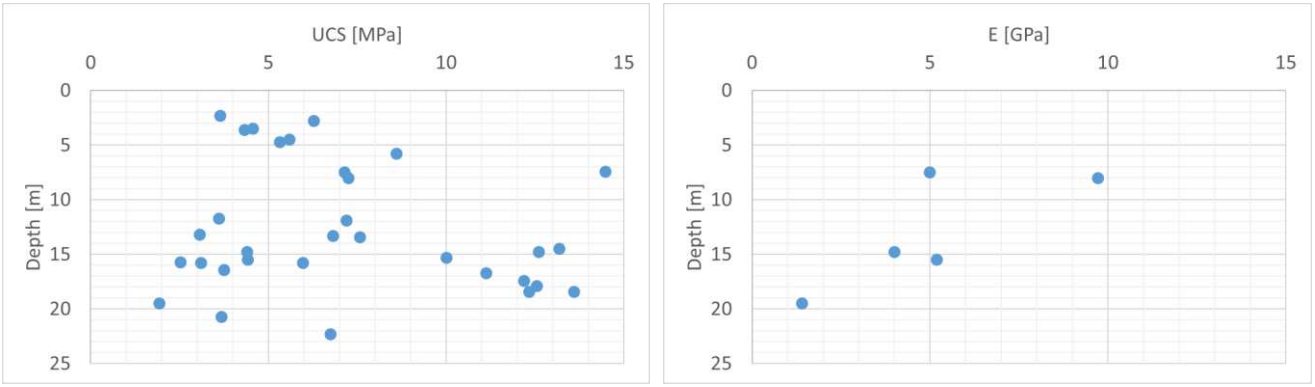

Figure 28. UCS and elastic modulus of laboratory tested elliptical jet grouting samples.

Stability Against Uplift (Permanent Micropiles)

To verify the design assumptions about the capacity of a permanent micropile embedded in an elliptical jet grouting column, an expendable, instrumented DCP bar was installed inside the test elliptical jet grouting column E-JG-2 (Figures 22 and 23). The jet grouting column was 7 m deep, 4 m long, and 1 m wide in plan (average width). The micropile was installed within a 250 mm diameter hole drilled for a depth of 6.5 m into the jet grouting column.

The maximum test load was 2,000 kN. The applied average shaft friction at the interface between the corrugated pipe to micropile (80 mm diameter corrugated PVC pipe) at the micropile-to-jet grouting interface (on the 250 mm diameter micropile shaft) and at the interface between the jet grouting column (considered with a 1 m x 4 m rectangular cross section) and soil were calculated using the values summarized in Table 1.

Table 1. Preliminary tensile load test on permanent micropile in elliptical jet grouting.

Test Load (kN)	Unit shaft friction on corrugated pipe (kPa)	Unit shaft friction on 250 mm diameter drill-hole (kPa)	Unit shaft friction on jet grouting column (kPa)
2000	1224	392	31

To monitor the strain development along the micropile shaft, two sets of vibrating wire miniature embedment strain gauges were installed at 4 levels along the DCP bar: at El. -6.00 m, El. -4.25 m, El. -2.50 m, and El. -0.75 m msl. For measuring the strain development inside the jet grouting column, two sets of 4 retrievable extensometers were installed at a distance of 0.5 m (EXT-B) and 1.5 m (EXT-A) from the micropile axis. Extensometers were inserted inside 51 mm diameter steel pipes, which were previously drilled and grouted. Two tell tale rods were used to measure the total pile estension and 14 displacement transducers (POTs) were needed to monitor the uplift at the surface at different locations. An automated digital survey level was used for monitoring the movement of the reference beam (precision of +/-0.01 mm) during the testing. Displacement, load, and strain data were automatically recorded at 30 second intervals. The main test geometry and general instrumentation layout are shown in Figures 29 and 30.

The testing was successfully conducted to the specified test load of 2,000 kN; however, several problems were encountered:

- To bring the surface of the jet grouting column above the groundwater table for conducting the test in dry condition, a 500 mm thick, clean concrete block was cast at the ground surface (Figures 29 and 30c). The lack of structural continuity and the considerable difference in stiffness between the jet grouting column and lean concrete affected most of the test readings of the displacement transducers at the surface.

- For the strain measurements during the testing, the miniature embedment type strain gauges didn't provide satisfactory results beginning at low levels of load due to the mobilized high tension strain concentrations.

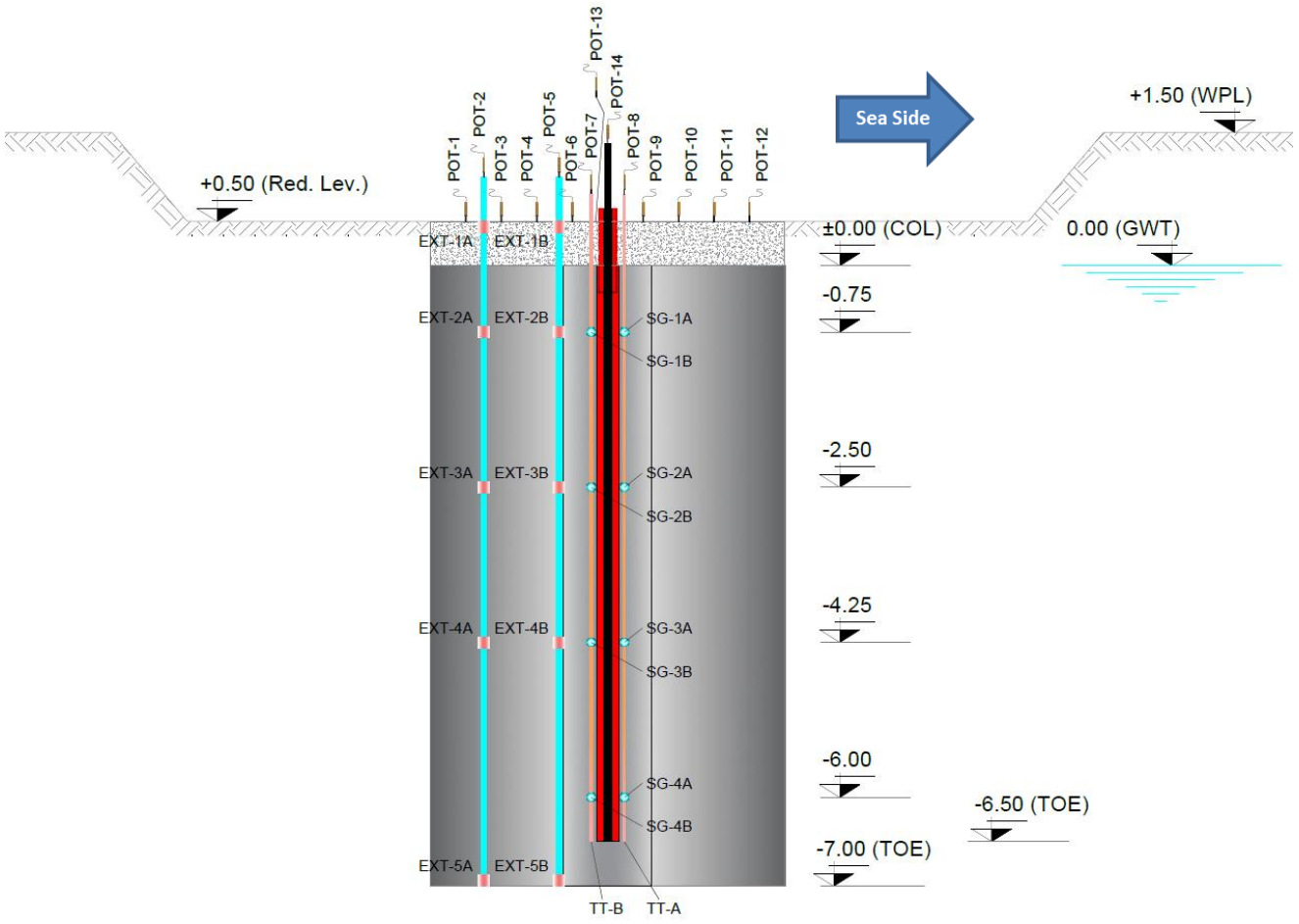

Figure 29. Main geometry of tension load test on DCP micropile.

(a)

(b)

(c)

Figure 30. (a) Exposed jet grouting column and preparation for drilling; (b) Installation of instrumented DPC bar, with visible vibrating wire miniature embedment strain gauges; and (c) General view of test set-up.

The results of head displacement showed a non-uniform uplift of the jet grouting column, which varied between 3.5 and 5.6 mm, while the maximum uplift measured on the DCP steel bar was 10.5 mm (Figures 31 and 32). This is possibly due to the irregular shape and mechanical properties of the jet grouting column or to the presence of lean concrete above the jet grouting.

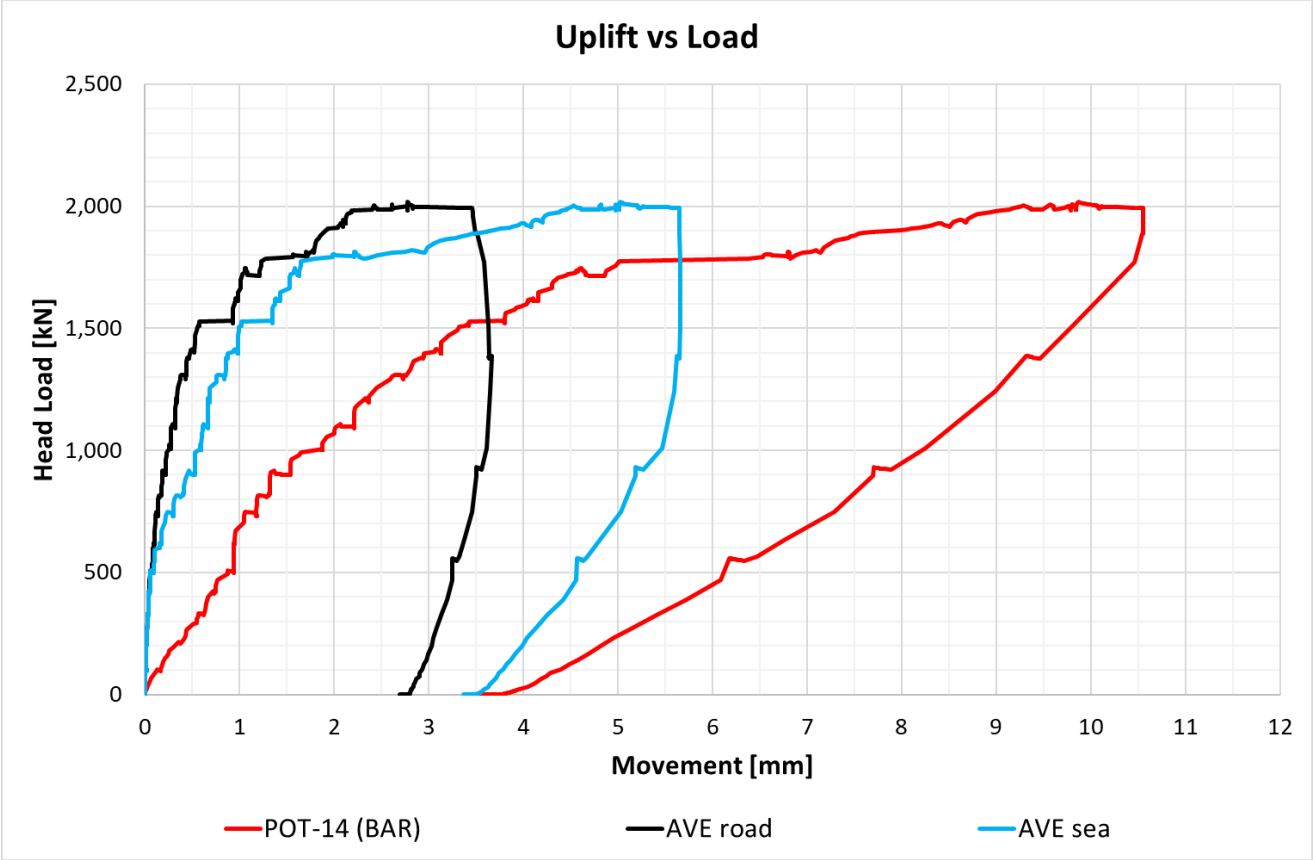

Figure 31. Tension load test results - Measured uplift.

It is possible to notice that concentrated surface cracks occurred at the load of 1800 kN (Figure 33).

As shown on Figure 34, the average total strain calculated from tell tales along the micropile was in line with the total strain values measured by extensometer EXT-B, even though the tell tales measurements showed a strange behavior that was most probably due to the vicinity of the DCP bar under tension. Therefore, the EXT-B strain values were considered for assessing the toe movement (Figure 35) and for the calculations of shaft friction and load distribution along the micropile and elliptical jet grouting column shafts. Given the significant dimensions in plan of the elliptical jet grouting column, it would be more correct to consider an average strain between the A and B extensometers for the jet grouting-to-soil shaft friction (Figure 36).

The load distribution (Figure 37) and relevant t-z curves along the micropile shaft (Figures 38 and 39) were calculated according to Fellenius et al (2000). It was possible to see that in the top portion of micropile near ground surface, the limit shaft friction is about 25 to 30 kPa and 300 to 350 kPa at the micropile-to-jet grouting interface and at the jet grouting-to-soil interface, respectively. At greater depths, the shaft friction values of 57 kPa and 720 kPa were achieved at micropile shaft and jet grouting shaft, respectively.

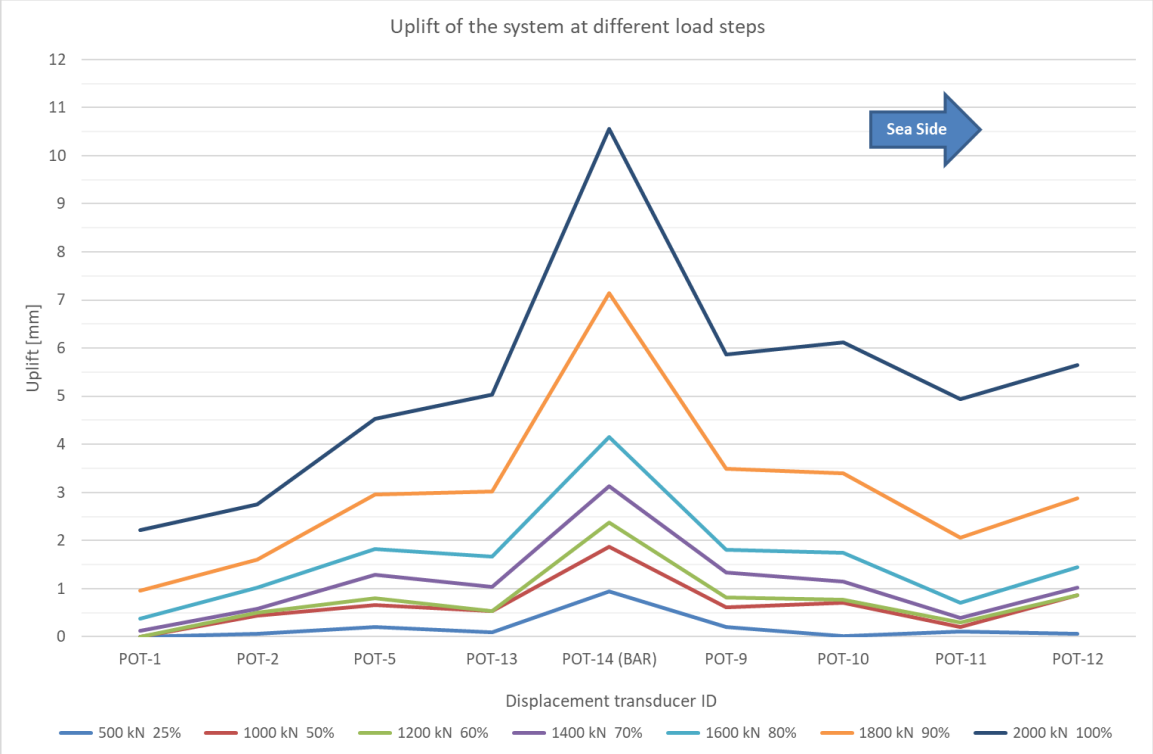

Figure 32. Uplift of elliptical jet grouting column and DCP bar at different load steps.

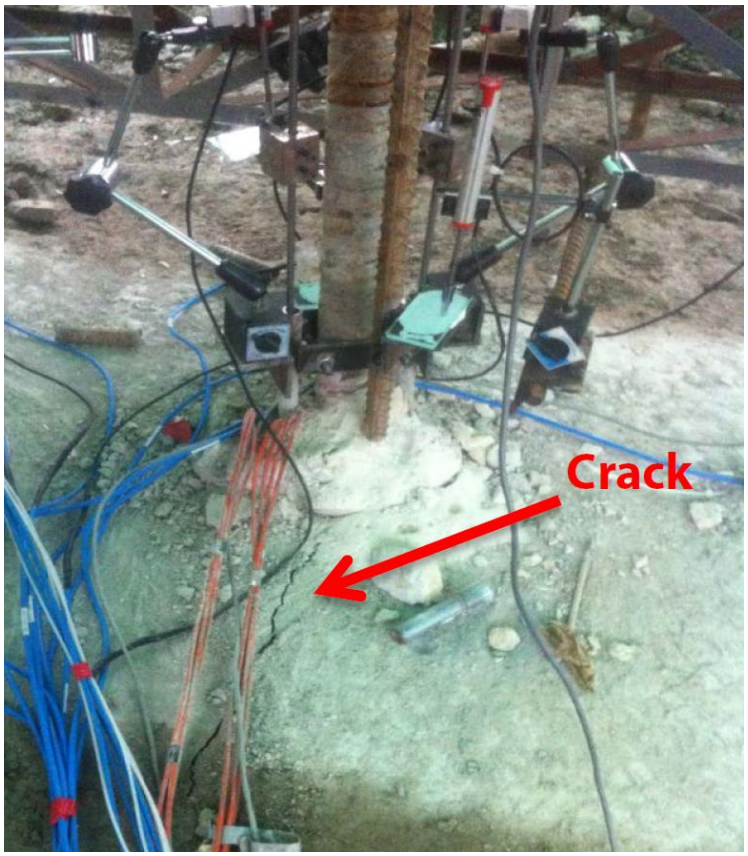

Figure 33. Surface crack development at 90% of test load (1800 kN).

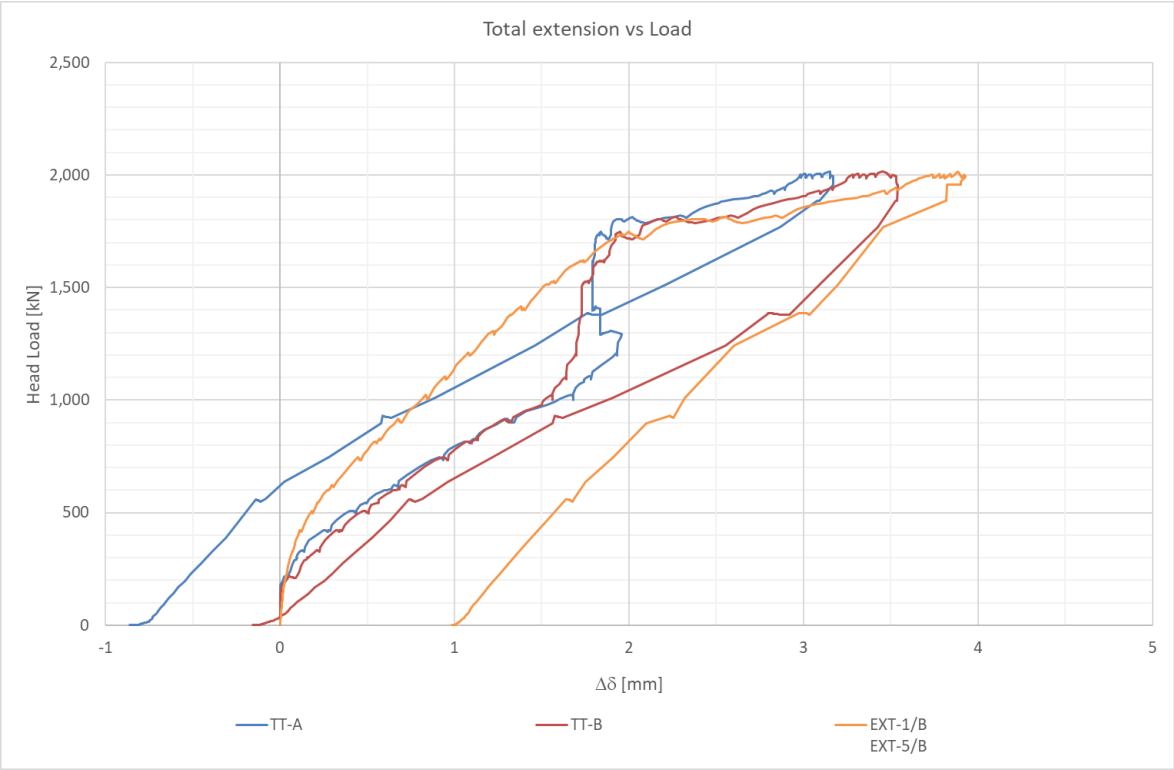

Figure 34. Total extension versus load.

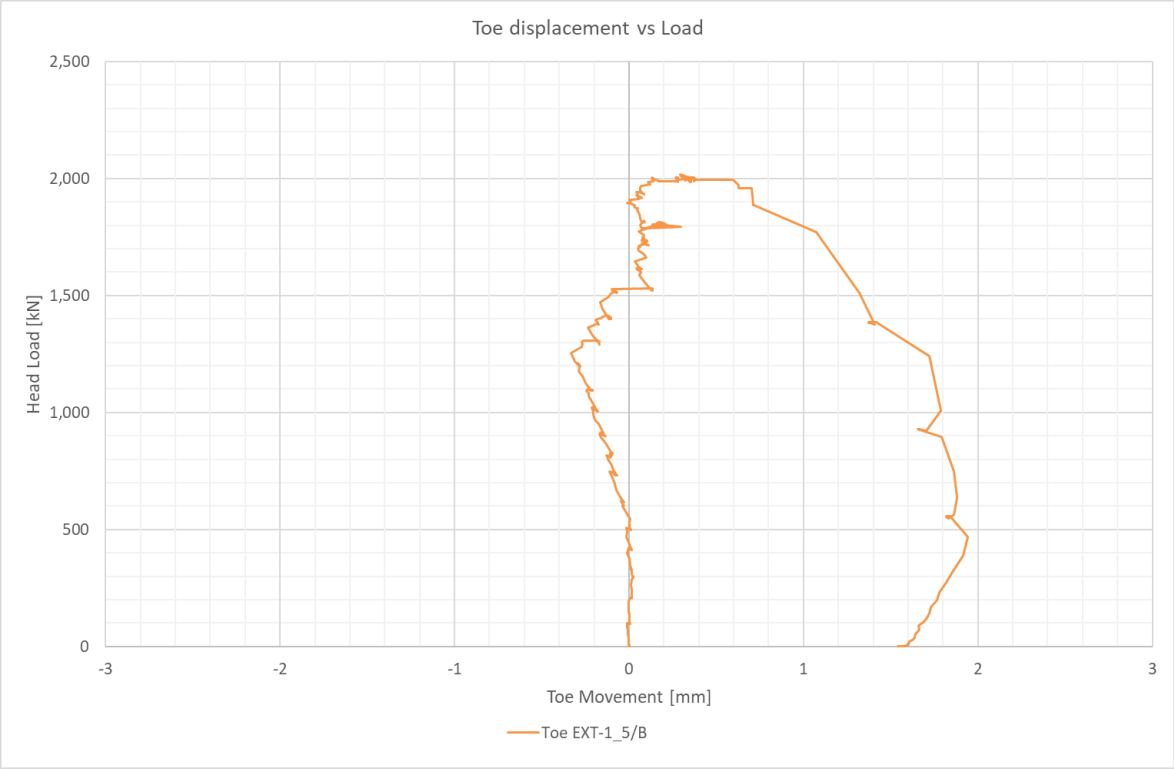

Figure 35. Toe movement versus load.

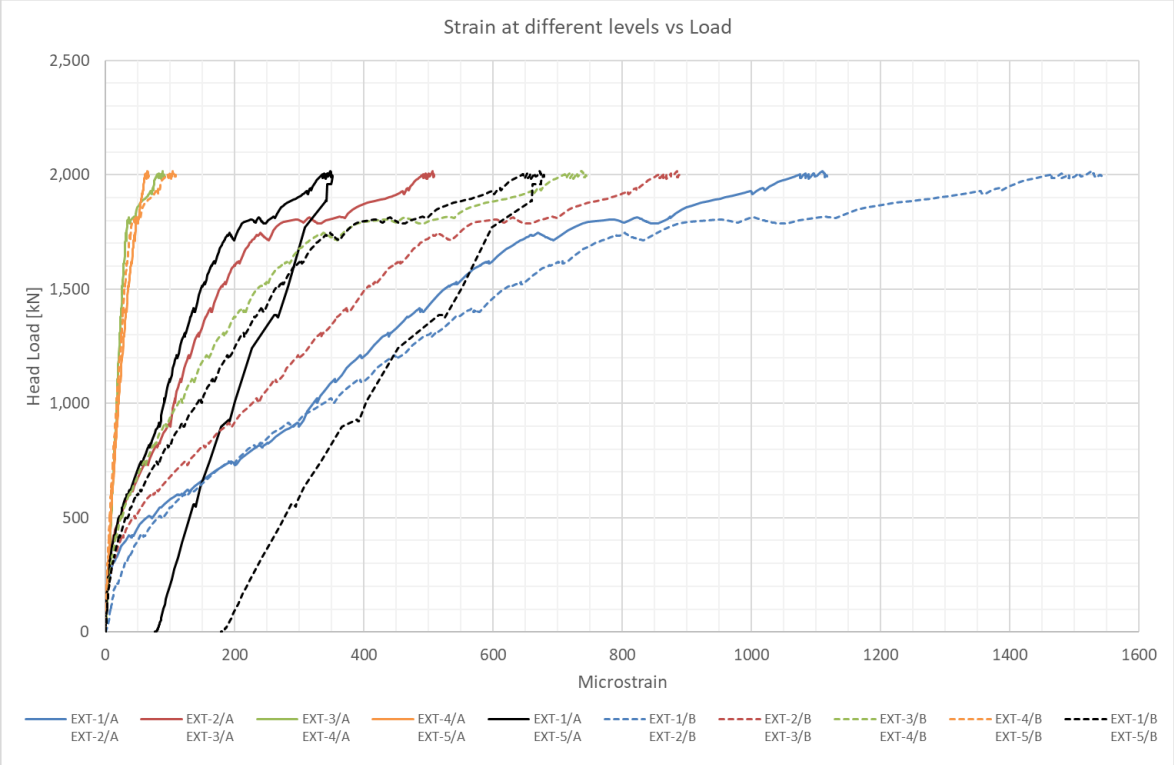

Figure 36. Average strain measured by the extensometers A and B.

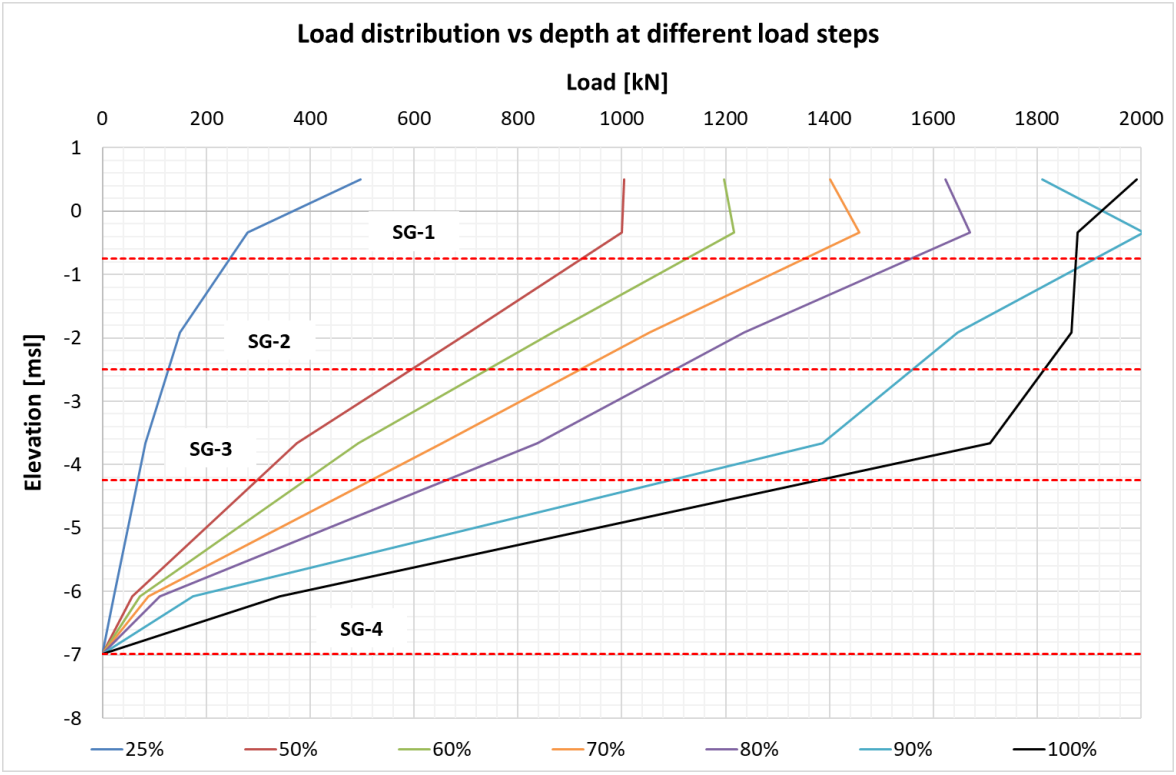

Figure 37. Load distribution at different load steps.

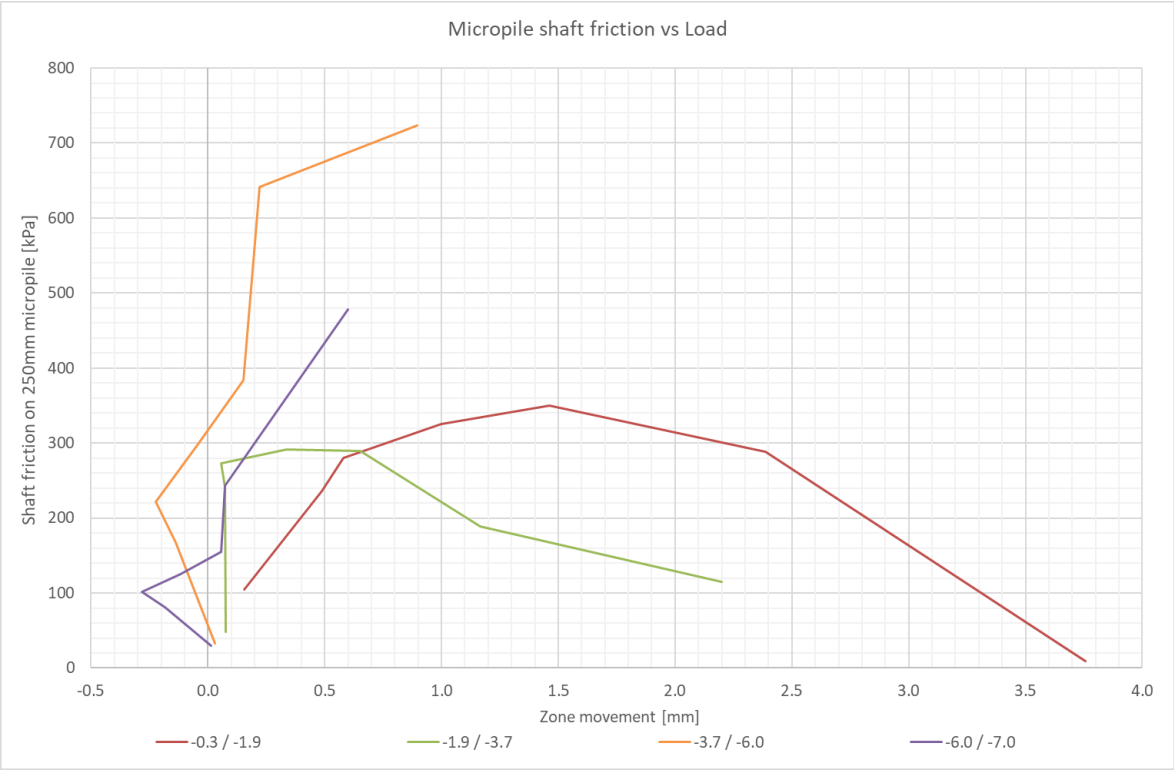

Figure 38. Micropile-to-jet grouting shaft friction vs zone movement.

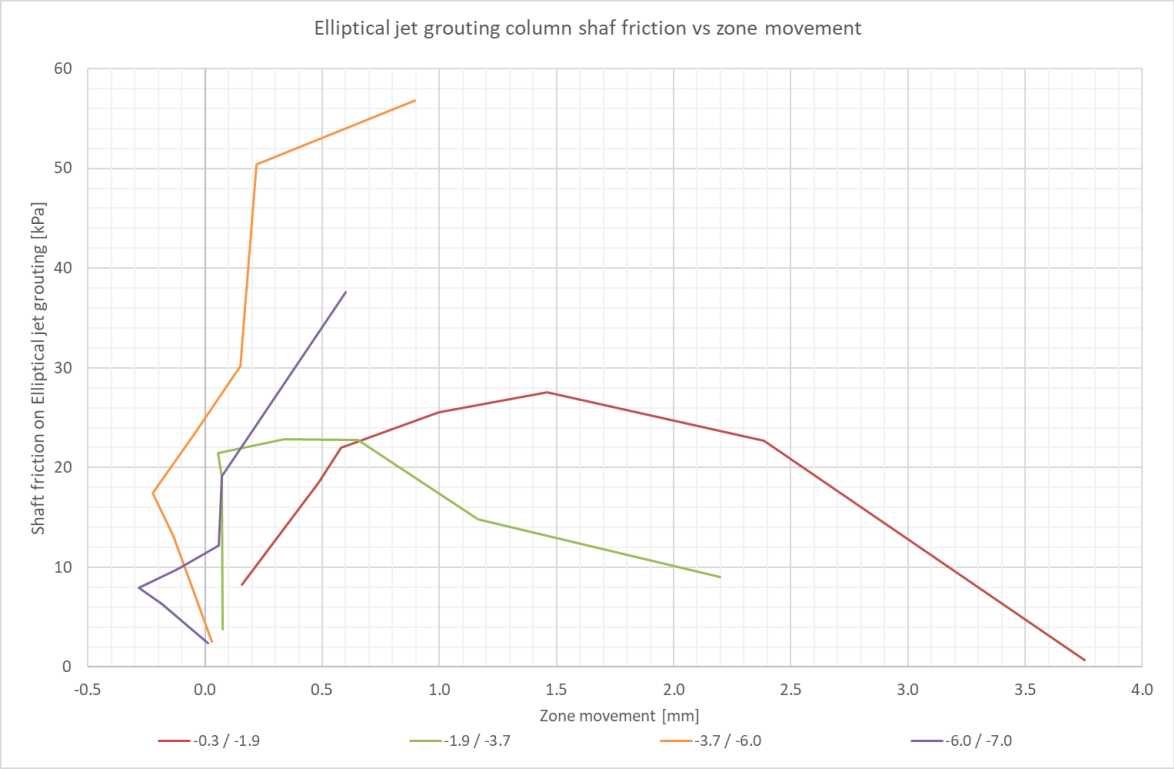

Figure 39. Jet grouting-to-soil shaft friction vs zone movement.

CONTROLS DURING PRODUCTION

The technologies involved and the electronic control devices employed for the execution of the MPBP are latest-generation. For the execution of the double fluid jet grout bottom plug, the drill rigs were equipped with the "Jet-Vision System" and with the "Drilling Position System" (DPS) electronic devices. The former controls and monitors the automatic rising of the drilling tool/rods during the jetting phase; the latter controls the 3D position of the drilling tool during the drilling phase, which is needed to ensure the overlapping between the jet grouting columns and the consequent successful execution of the bottom plug. The DPS conists of an inclinometer attached to the bottom of a drilling rod string, which takes readings at pre-determined depths (usually every 0.5 m to 1.0 m) during the drilling process. Recorded deviation data are downloaded at the end of each executed jet grouting column. As an example, the measured frequency distribution of vertical deviation is shown in Figure 40 and has a median of 1.41 % and a standard deviation of 1.33 %.

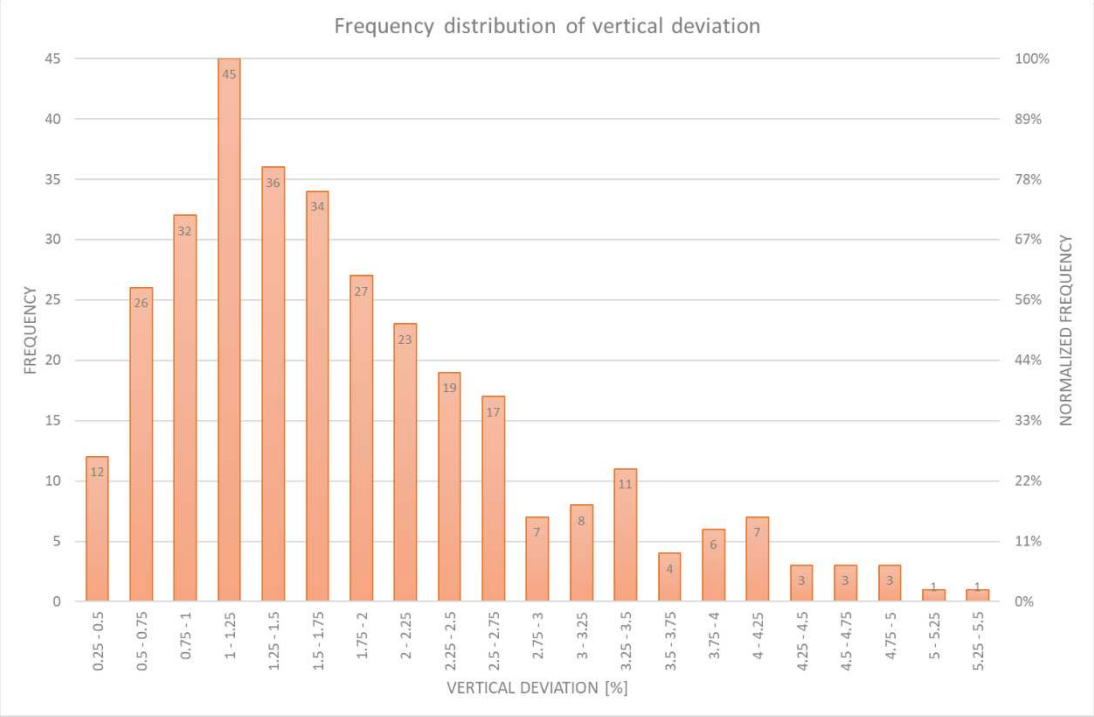

Figure 40. Frequency distribution of vertical deviation during drilling, measured with DPS.

For the execution of the pseudo-elliptical jet grout columns, the Jet-Vision System was provided with the "orbital jet" option, which allows the user to modify the rotation speed during the jetting phase in a planned way. The DPS was also used during the execution of both elliptical jet grout columns and the DCP micropiles. This allowed the driller to locate the jet grout columns at the bottom of the excavation (shown in blue in Figure 41) and at the bottom end of the columns (shown in magenta in Figure 41) and to make sure that DCP micropiles (shown in red in Figure 41) were always installed within the jet grout columns. This was important since the micropiles had been designed to be "fully embedded in elliptical jet grouting," considering an ultimate micropile-to-jet grouting skin friction of 400 kPa. Taking into account that all activities were executed from the original working platform prior to the start of excavation, the correct position of micropiles could not be ensured by visual inspection and had to rely on the executed DPS measurements.

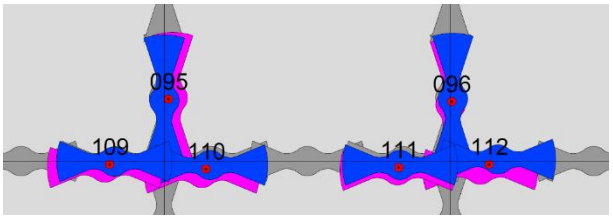

Figure 41. As-built elliptical jet grouting and DCP micropiles by using DPS.

FINAL QA/QC CONTROLS

Final tests were conducted on each of the three executed activities (i.e., bottom plug, lattice-type soil improvement, and DCP micropile) to guarantee the correct execution according to the design requirements.

Seepage Control (Double Fluid Jet Grouting)

To assess the quality of the executed jet grouting bottom plug and to estimate its equivalent hydraulic conductivity, an in-situ, in-scale pumping test was conducted. The main scope of the pumping test was to assess the water flow entering the system (Q_{in}) in a given condition, which was then used to estimate the equivalent permeability of the bottom plug (k_{BP}).

$$Q_{in} = k_{BP} \times i \times A_{BP} \Rightarrow k_{BP} = \frac{Q_{in}}{i \times A_{BP}} \quad (8)$$

where:

Q_{in} Water inflow (l/s);

i ydraulic gradient (Δ_h / H_{BP}), where Δ_h is the hydraulic load and H_{BP} is the thickness of bottom plug; and

A_{BP} Surface in plan of bottom plug.

Five deepwells and four piezometers were installed in the Bina 4 excavation area (Figure 42). In reality, the ingress of water can happen through the whole system consisting of the jet grout bottom plug, secant piles, and diaphragm wall; however, it is assumed that the surrounding shoring is almost watertight and that the water inflow affects mainly the bottom plug.

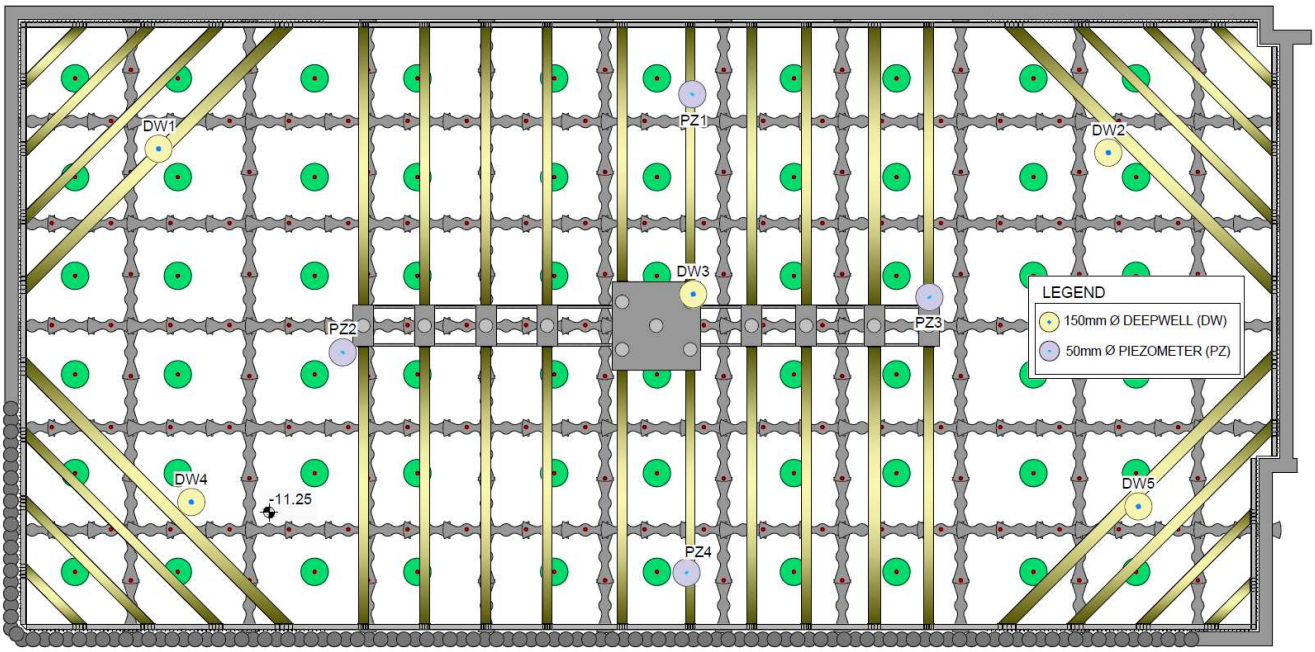

Figure 42. Pumping test layout.

In Equation (1), the main unknown is the water inflow Q_{in}, which can be assessed by analysing the drawdown and recharge process of the conducted pumping test. The following conditions were observed:

- During drawdown phase (pumping stage), in a given time interval, the difference between the volume of water that is pumped out (V_{out}) and the one that enters the system (V_{in}) generates a variation in the water level measured inside the shoring system (Δh_d).
- During the recharge phase, in a given time interval, the volume of water that enters the system generates a variation of water level measured inside the shoring system (Δh_r).

where:

Q_{out} Pumping water discharge (l/s);

n Porosity of soil in pumping area (%);

Δh_d Hydraulic load in drawdown stage (m);

Δh_r Hydraulic load in recharge stage (m);

Δt_d Time interval in drawdown stage (s); and

Δt_r Time interval in recharge stage (s).

These two conditions can be written in a system of two equations (9), which can be solved with respect to the two unknowns Q_{in} and (n x A_{BP}) as listed in Equation (10).

$$\begin{cases} DRAWDOWN \Rightarrow (V_{out} - V_{in}) = \Delta V \Rightarrow (Q_{out} - Q_{in}) \times \Delta t_d = (n \times A_{BP}) \times \Delta h_d \\ RECHARGE \Rightarrow Q_{in} \times \Delta t_r = (n \times A_{BP}) \times \Delta h_r \end{cases} \quad (9)$$

$$\begin{cases} (n \times A_{BP}) = \frac{Q_{out} \times \Delta t_d \times \Delta t_r}{(\Delta t_d \times \Delta h_r + \Delta t_r \times \Delta h_d)} \\ Q_{in} = \frac{\frac{Q_{out} \times \Delta t_1 \times \Delta t_2}{(\Delta t_d \times \Delta h_r + \Delta t_r \times \Delta h_d)} \times \Delta h_r}{\Delta t_r} \end{cases} \quad (10)$$

Once Q_{in} is calculated, it can be used in Equation (8) to assess the equivalent permeabilty of the bottom plug.

The drawdown phase was run from 9 to 14 October 2017, and the groundwater table was lowered from the original El. 0.00 msl to around El. -5.0 msl. The recharge phase followed. In addition to the manual readings, the water level in three deepwells (DW-1-3-4) and three piezometers (PZ-1-3-4) was automatically measured by means of level loggers. The two phases can be separated and the trendlines generated. The manual and automatic readings taken during the drawdown phase are shown in Figures 44 and 45 and relevant trendlines have an average slope of -1 m/day, showing that for every one day period, there is a 1 m drop in water level. During the recharge phase, a slope between 0.05 and 0.07 m/day was measured with manual readings (Figure 46), while 0.10 to 0.12 m/day was measured by the automatic level logger (Figure 47).

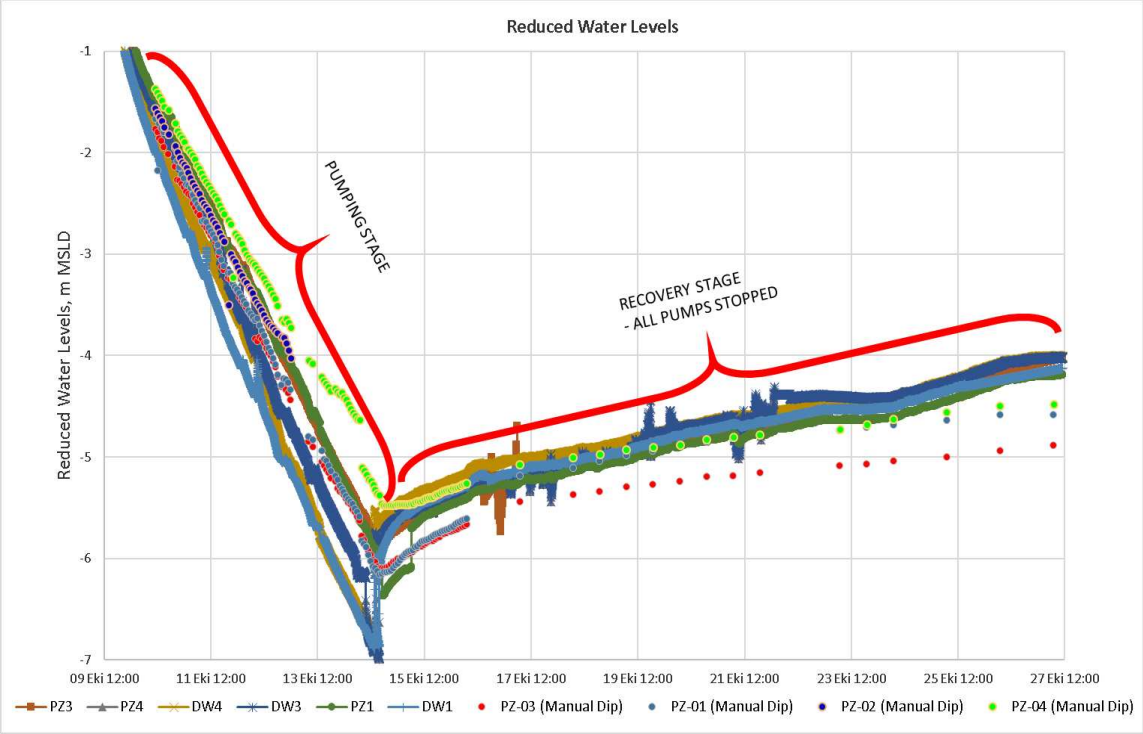

Figure 43. Water levels during pumping test.

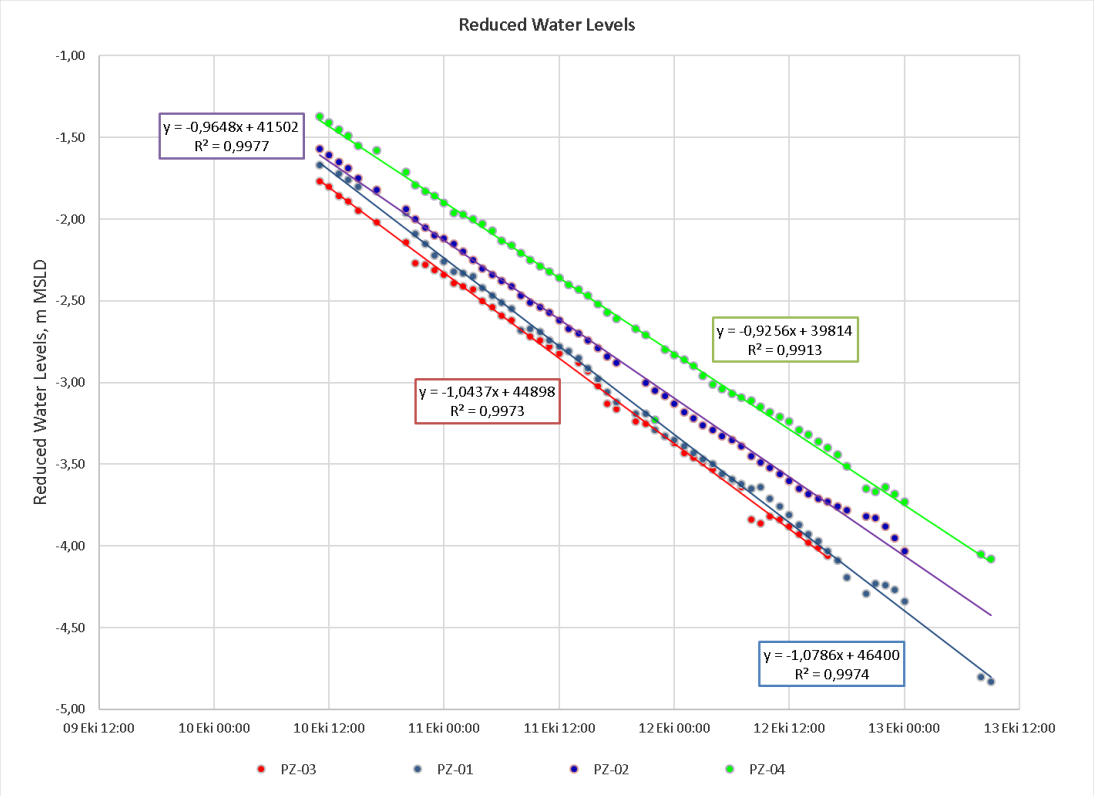

Figure 44. Graph of Manual Dipmeter Readings in Drawdown Stage.

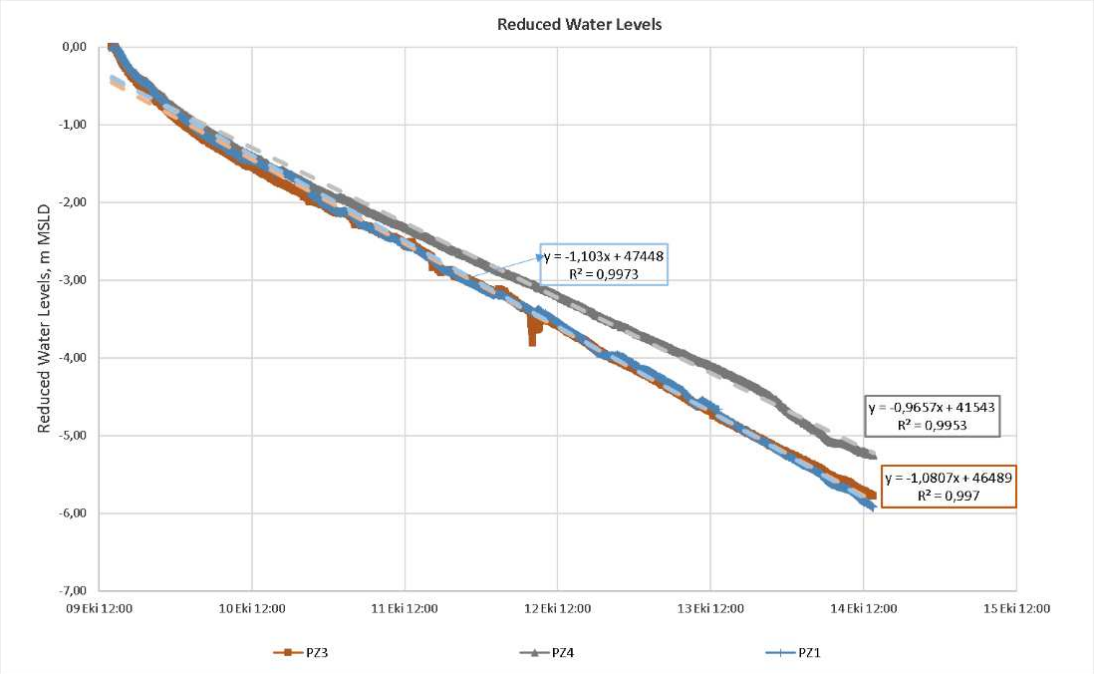

Figure 45. Graph of Automatic Levellogger Readings in Drawdown Stage.

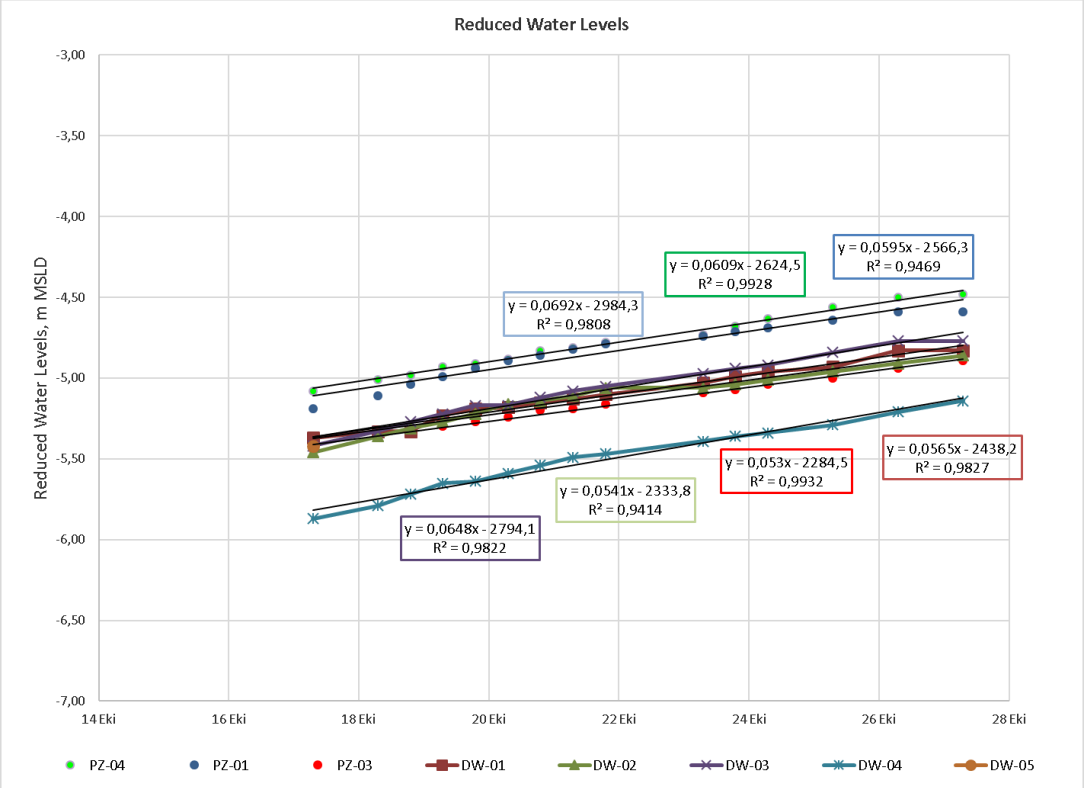

Figure 46. Graph of Manual Dipmeter Readings in Recovery Stage.

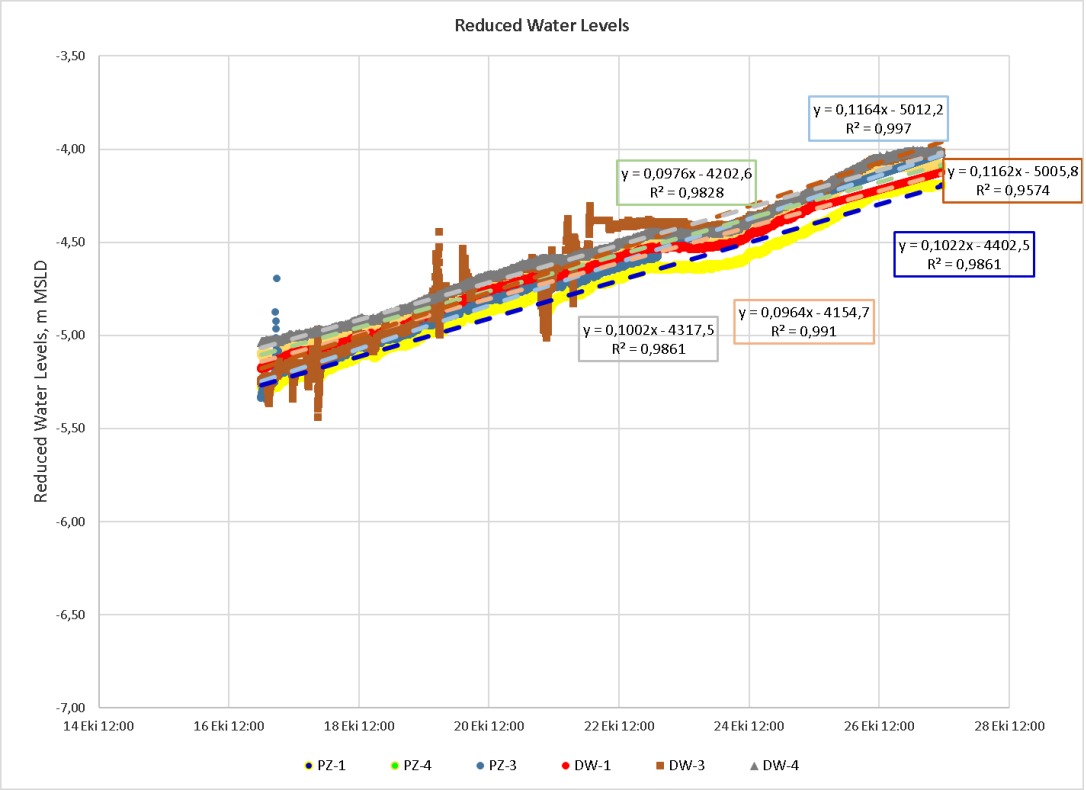

Figure 47. Graph of Automatic Levelloger Readings in Recovery Stage.

Based on the above readings, the considered average drawdown rate $\Delta h_d / \Delta t_d$ is 1 m/day, while the considered average recharge rate $\Delta h_r / \Delta t_r$ is 0.12 m/day, for safety reasons. Using these two values in Equation (10), the inflow of 1.07 l/s was calculated.

$$Q_{in} = \frac{\frac{10\ l/s \times 1\text{day} \times 1\ \text{day}}{(1\ \text{day} \times 0.12\ \text{m}/day + 1\ \text{day} \times 1\ \text{m}/day)} \times 0.12\ \text{m}/day}{1\ \text{day}} = 1.07\ l/s \quad (11)$$

The hydraulic gradient was calculated to be as shown in Equation (12).

$$i = \frac{\Delta h}{H_{BP}} = \frac{5\ m}{3.5\ m} = 1.43 \quad (12)$$

Equation (8) can be used to assess the equivalent hydraulic conductivity of the jet grouting bottom plug, as shown in Equation (13).

$$k_{BP} = \frac{Q_{in}}{i \times A_{BP}} = \frac{0.00107\ m^3/s}{1.43 \times 3200\ m^2} \approx 2.5 \times 10^{-7} m/s \quad (13)$$

If the value k_{BP} = 2.5 x 10^{-7} m/s is compared with the 10^{-4} m/s of the in-situ sand in original condition, it means that a reduction of permeability greater than 400 times was obtained by means of installing the jet grout bottom plug. The estimated value of hydraulic conductivity was also used to assess the total water flow expected at the bottom of excavation level of El. -11.15 msl.

$$Qf_{in} = k_{BP} \times \frac{\Delta h_{fin}}{H_{BP}} \times A_{BP} = \approx 2.5 \times 10^{-7} m/s \times \frac{11.5\ \text{m}}{3.5\ \text{m}} \times 3200\ \text{m}^2 = 2.6\ l/s \quad (14)$$

The actual records of water outflow were obtained at the bottom of excavation range between 2 and 5 l/s, with a median value of 3 l/s (Figure 48), which is in good agreement with the preliminary calculations.

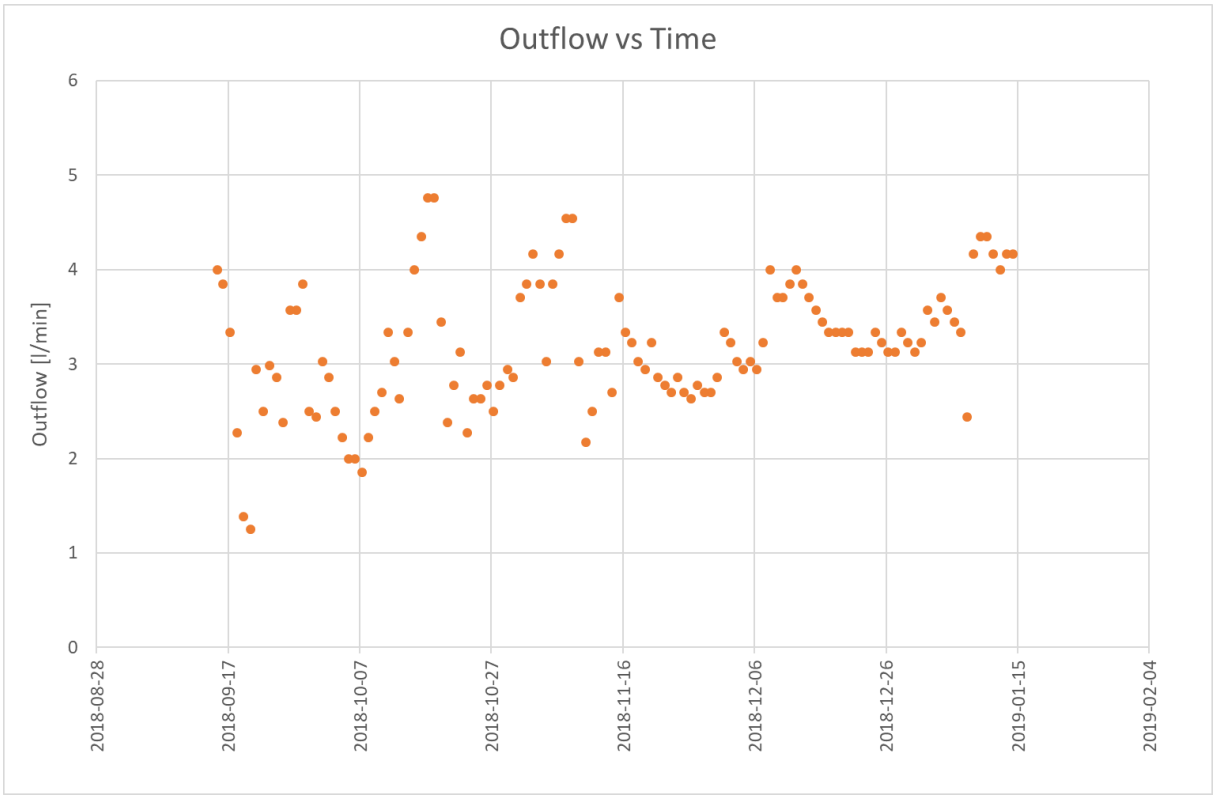

Figure 48. Recorded total outflow at bottom of excavation.

Two rotary core drillings up to a depth of 25 m were performed as quality control checks on the executed jet grout columns between 2 and 6 June 2017 in Bina 4. Samples were taken from both boreholes to test them in the laboratory. Quality control corings were executed in the overlapping of two adjacent columns: B-41 and B-42 (type B = 4 m long in plan) as well as A-60 and A-61 (type A = 3.5 m long in plan).

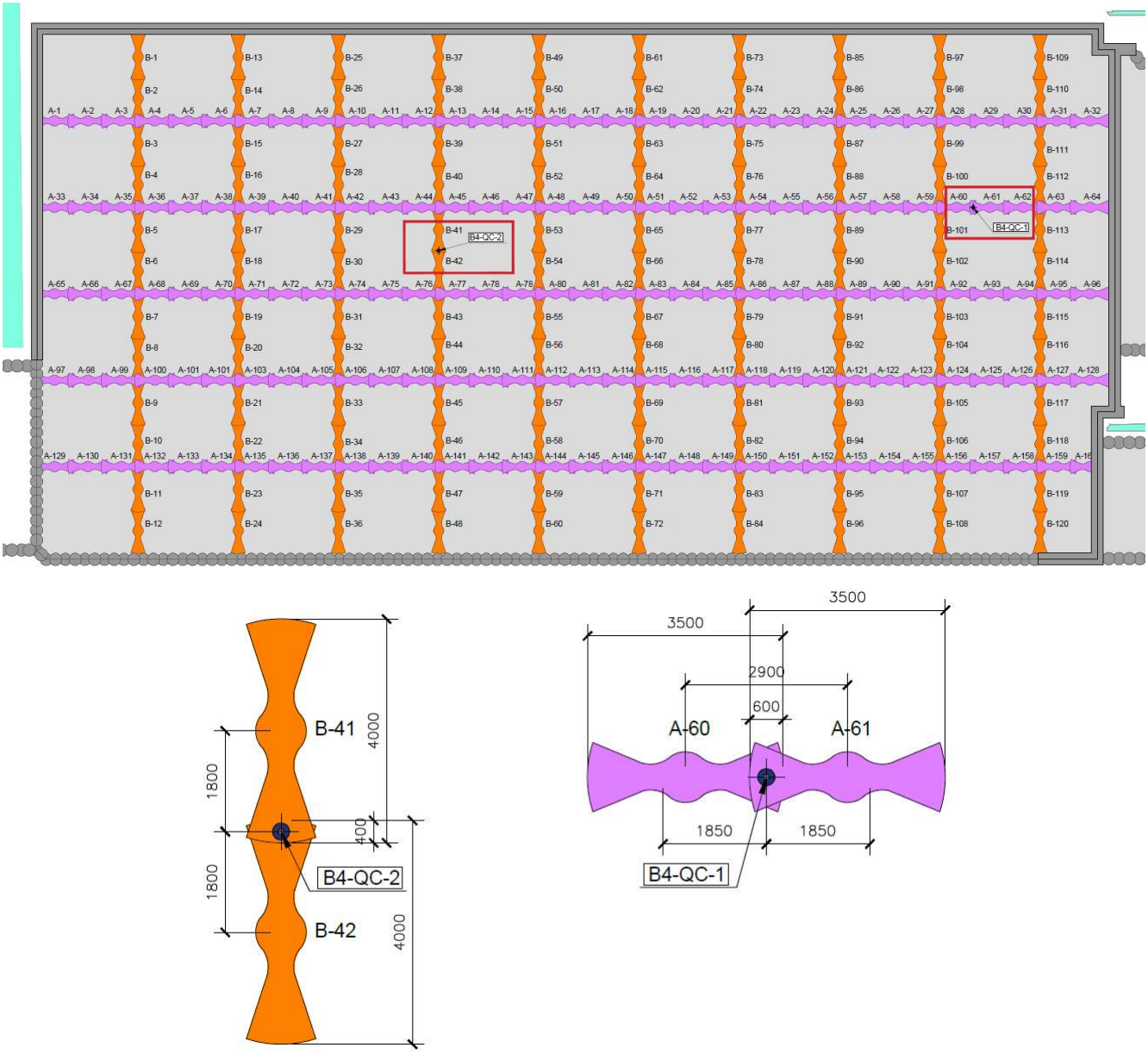

Figure 49. Details of corings with respect to executed columns.

For both cores, full core recovery was obtained (Figure 50), which confirm a satisfactory quality of the soil improvement and a continuous overlapping between two adjacent columns. As also shown in Figure 50, the samples selected for laboratory testing are highlighted by a red rectangle. The cylinders (100 mm x 200 mm) were prepared and tested to determine the UCS and elastic modulus. The average value of UCS was 6.43 MPa and the average Es was 8.79 GPa. Both values were greater than the specified 5 MPa and 5 GPa for UCS and Es, respectively.

Table 2. Summary of UCS and Es values measured on eliptical jet grouting samples.

Core ID	Sample ID	Elastic Modulus (MPa)	Unconfined Compressive strength (MPa)
B4-QC-1	CSS1	8,325	7.68
B4-QC-1	CSS2	14,231	8.30
B4-QC-1	CSS3	8,344	7.27
B4-QC-1	CSS4	7,124	3.96
B4-QC-1	CSS5	8,470	5.33
B4-QC-1	CSS6	11,073	5.93
B4-QC-2	CSS1	8,620	5.96
B4-QC-2	CSS2	12,898	10.53
B4-QC-2	CSS3	10,652	8.04
B4-QC-2	CSS4	1,503	2.60
B4-QC-2	CSS5	5,504	5.18

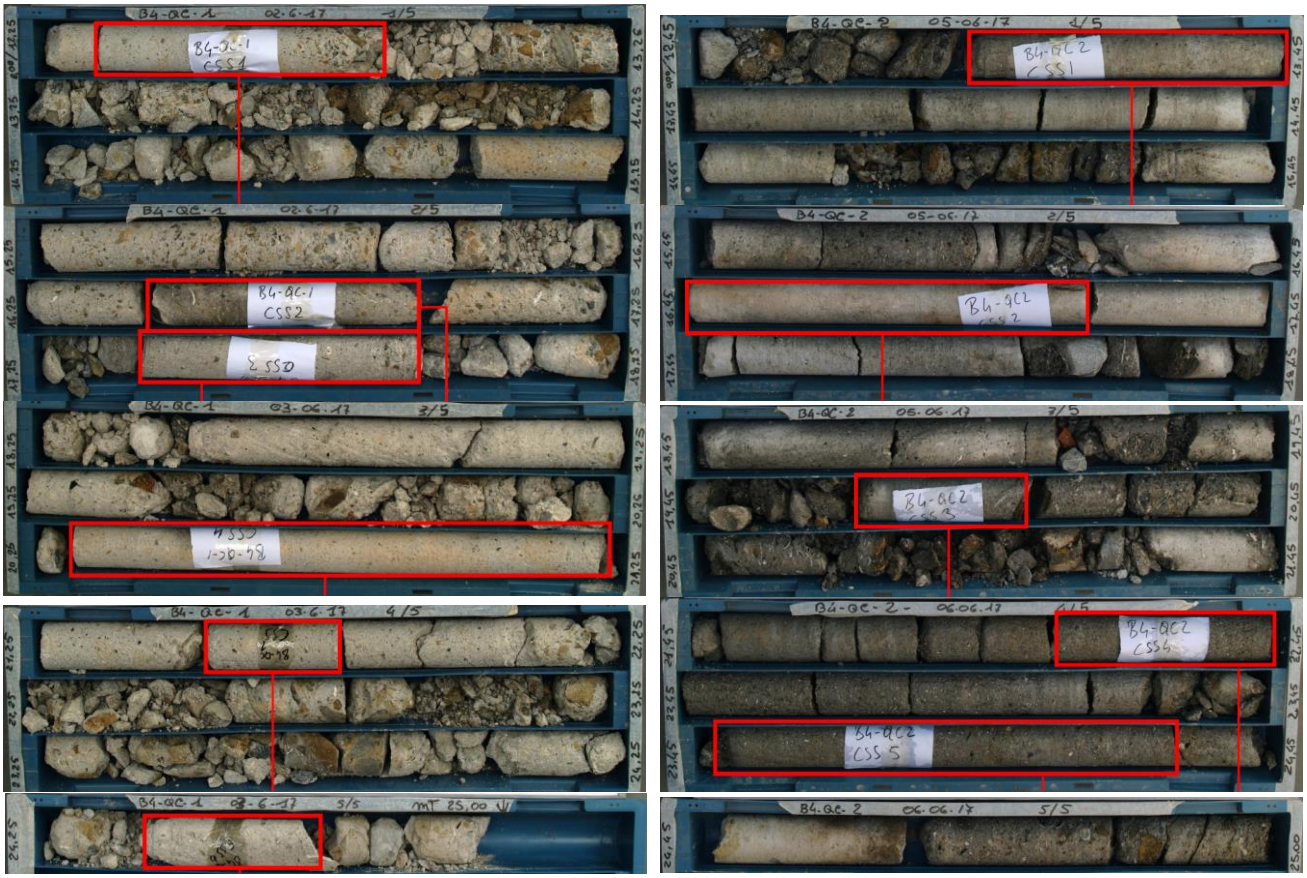

(a) *(b)*

Figure 50. Core box photos of executed continuous coring: (a) QC-1 and (b) QC-2.

The different quality of the cores at different depths might be related to the heterogenous nature of the man-made fill.

Stability Against Uplift (Permanent Micropiles)

Once the final excavation level was reached, all permanent micropiles were subjected to acceptance testing up to 125% of the design working load (test load of 1,731 kN and design working load of 1,385 kN) to evaluate the micropile response. The typical acceptance test arrangement is shown in Figure 51.

Figure 51. Typical arrangement of acceptance test.

The micropiles were loaded from the datum (P_a) load to proof load (P_p) in three increments: 50%, 100% (P_w), and 125% (P_p) of working load (P_w). The proof load was maintained for 15 minutes. Readings were recorded at 1 minute intervals at 50% and 100% (P_w) and at 1, 2, 3, 4, 7, and 15 minutes at 125% (P_p). The micropiles were unloaded from the proof load (P_p) to 100% (P_w), = then to 50%, and then to the datum load (P_a). Readings were recorded at 1 minute intervals at each step during unloading. Graphs of load vs. displacement for each of the tested micropiles are shown in Figure 52. The uplift under the maximum test load of 1731 kN ranged between 1.8 mm and 18.4 mm, with a median value of 6.15 mm. The median micropile response is shown in thick red lines in Figure 52.

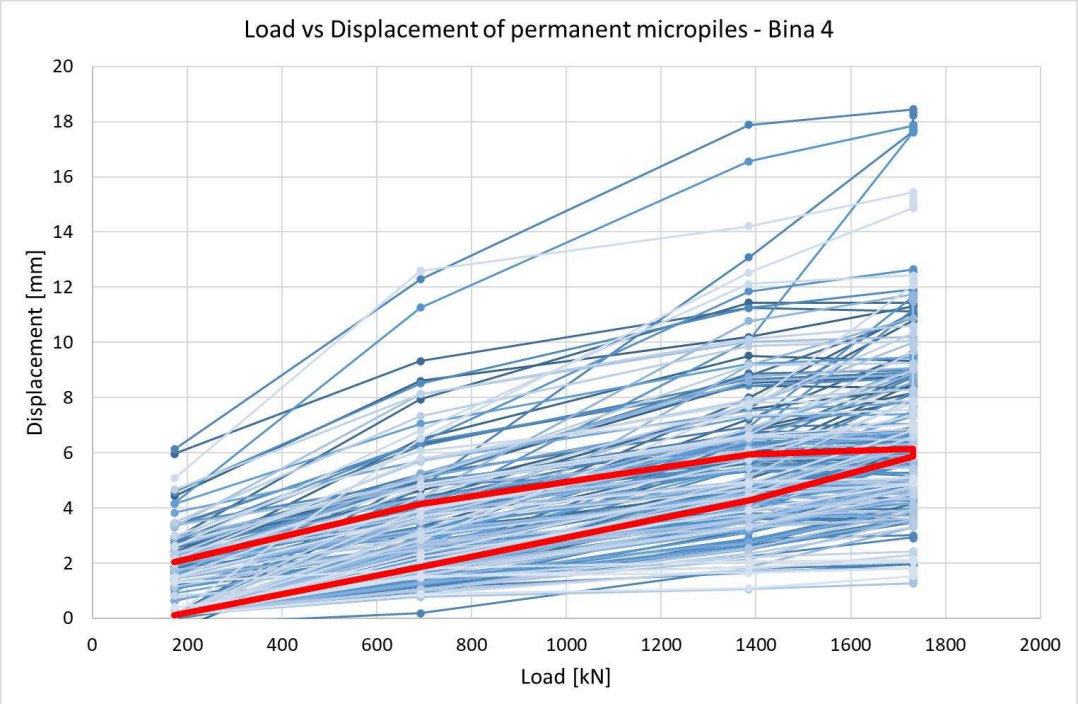

Figure 52. Load – Displacement graph of all tested micropiles.

DISCUSSION AND CONCLUSION

The multi-purpose bottom plug (MPBP) is an innovative geotechnical solution which combines seepage control, ground improvement against liquefaction, and load bearing elements. It was adopted to allow the deep excavation of a 3-basement building (12.5 m depth, 11.0 m below the sea level). For this project, the main elements of the MPBP include:

- Seepage Control: Bottom plug formed by overlapping jet grouting circular columns (2,000 mm diameter, double-fluid), executed on a triangular pattern with an average center-to-center spacing of 1500 mm.
- Liquefaction Risk Mitigation: Pseudo-elliptical jet grouting columns on a lattice-type pattern. Average width of columns is 4.0 m.
- Stability Against Uplift: Permanent 63.5 mm double corrosion protected steel bars, installed in drilled 250 mm diameter holes and grouted micropiles through the previously-executed elliptical jet grouting.

The key lessons learned from this experience can be summarized as follows:

- The MPBP is proof that a combination of different technologies can be used to solve several problems simultaneously by optimizing the application of a single technology and by reducing the relevant time and cost of the project.
- It is important to perform an extensive and exhaustive soil investigation campaign for the design of a soil improvement intervention. This is generally true for all geotechnical engineering problems, but it is even more important in the presence of a man-made fill or for projects located in a coastal area where the soil conditions might vary substantially even within a few tens of meters.
- The design required the use of advanced geotechnical analysis and design software. The design of the MPBP was carried out using a non-linear time history 3D FDM analysis using FLAC3D.
- Cutting-edge technologies within the foundation engineering field, like the pseudo-elliptical jet grouting, required the use of the latest and sophisticated drilling rigs.
- The use of state-of-the-art electronic control devices facilitated the operation and maintained the required accuracy needed.
    - The Jet-Vision System controlled and monitored the automatic rising of the drilling tool/rods during the jetting phase and, due to the orbital jet option, it was possible to automatically modify the rotation speed during the jetting phase in a planned way for the pseudo-elliptical jet grouting.
    - The Drilling Position System monitored the 3D position of both the jet grouting columns and micropiles, which was important for the successful execution of the bottom plug and for making sure that micropiles were installed within the previously-executed jet grouting columns.
- The preliminary field test on the elliptical jet grouting confirmed that it was possible to obtain elliptical jet grouting columns up to 4.0 – 4.5 m wide in plan, if the soil conditions are favorable (i.e., very loose sand).
- A ratio of about 1,300 was found between the elastic modulus and the unconfined compressive strength of cylinder samples taken from executed elliptical jet grouting columns (Es = 8.8 GPa, UCS = 6.4 MPa).
- The preliminary pull out test on the DCP bar confirmed that it was possible to design the jet grouting columns as structural elements. However, a greater safety factor should be considered taking into account the intrinsic heterogeneity of the improved soil. In the present case, the jet grout columns were used as bearing elements for tension micropiles, and an ultimate micropile-to-jet grouting shaft friction greater than 400 kPa was obtained.
- During the preliminary pull out test of the DCP bar, the vibrating wire miniature embedment strain gauges didn't provide a satisfactory performance beginning at low levels of load, most probably due to the mobilized high tension strain concentrations. It is recommended to use retrievable extensometers in this type of test, if possible.
- The executed jet grout bottom plug reduced the natural hydraulic conductivity of the in-situ sand by about 400 times from 10^{-4} m/s to 2.5 x 10^{-7} m/s.
- The in-situ pumping test executed prior to starting the bulk excavation at the site was a great way to estimate the global hydraulic conductivity of the shoring-bottom plug system.

- Since all activities were carried out from the existing ground level, which was almost 12 m above the bottom of excavation, it was very difficult to ensure that DCP micropiles were installed in the middle of the elliptical jet grouting column. Many drill holes were repeated to center the hole. If this solution will be applied again in the future, it would be recommended to work from a working platform that would be close to the micropile cutoff level. This way, the empty drilling length would be reduced and the drilling deviation would be better controlled.
- The Drilling Position System didn't always have satisfactory results because the instrument is attached to the the string of drilling rods and is subject to vibrations and impacts during drilling. In some cases, the deviation readings couldn't be obtained. An alternative method was also tried at the site, using the shape-accelerometer array (SAA). The use of SAAs is recommended for measurements of drilling deviations.
- Expertise played a pivotal role for the correct execution of the MPBP and for the successful completion of this high profile project.

ACKNOWLEDGMENTS

The author appreciated the continuous assistance provided by Galataport (client) and ENAR (client's geotechnical consultant). At the design stage, the collaboration between the TREVI R&D office and ITASCA was also important for the detailed analysis and design of the MPBP, while the support of GEOGRUP was fundamental for the correct execution of the onsite micropile load testing and coring.

REFERENCES

Takahashi H., Yamawaki S., Kitazume M. and Ishibashi S. (2006). *Effects of deep mixing method on liquefaction prevention and proposal on new arrangement of grid-type improvement*, Report of the Port and Airport Research Institute, 45(2), 135-167. (in Japanese).

Namikawa T., Koseki J. and Suzuki Y. (2007). "Finite element analysis of lattice-shaped by ground improvement by cement-mixing for liquefaction mitigation." *Soils and foundations (Japanese Geotechnical Society),* 47(3), 559-576.

Takahashi H., Morikawa Y., Iba H., Fukada H., Maruyama K. and Takehana K. (2013). "Experimental study on lattice-shaped cement treatment method for liquefaction countermeasure." *Proc. of the 18th International Conference on Soil Mechanics and Geotechnical Engineering*, Paris.

Fellenius, B.H., Brusey, W.G., and Pepe, F. (2000). "Soil Set-up, Variable Concrete Modulus, and Residual Load for Tapered Instrumented Piles in Sand." *American Society of Civil Engineers, ASCE, Specialty Conference on Performance Confirmation of Constructed Geotechnical Facilities*, University of Massachusetts, Amherst.

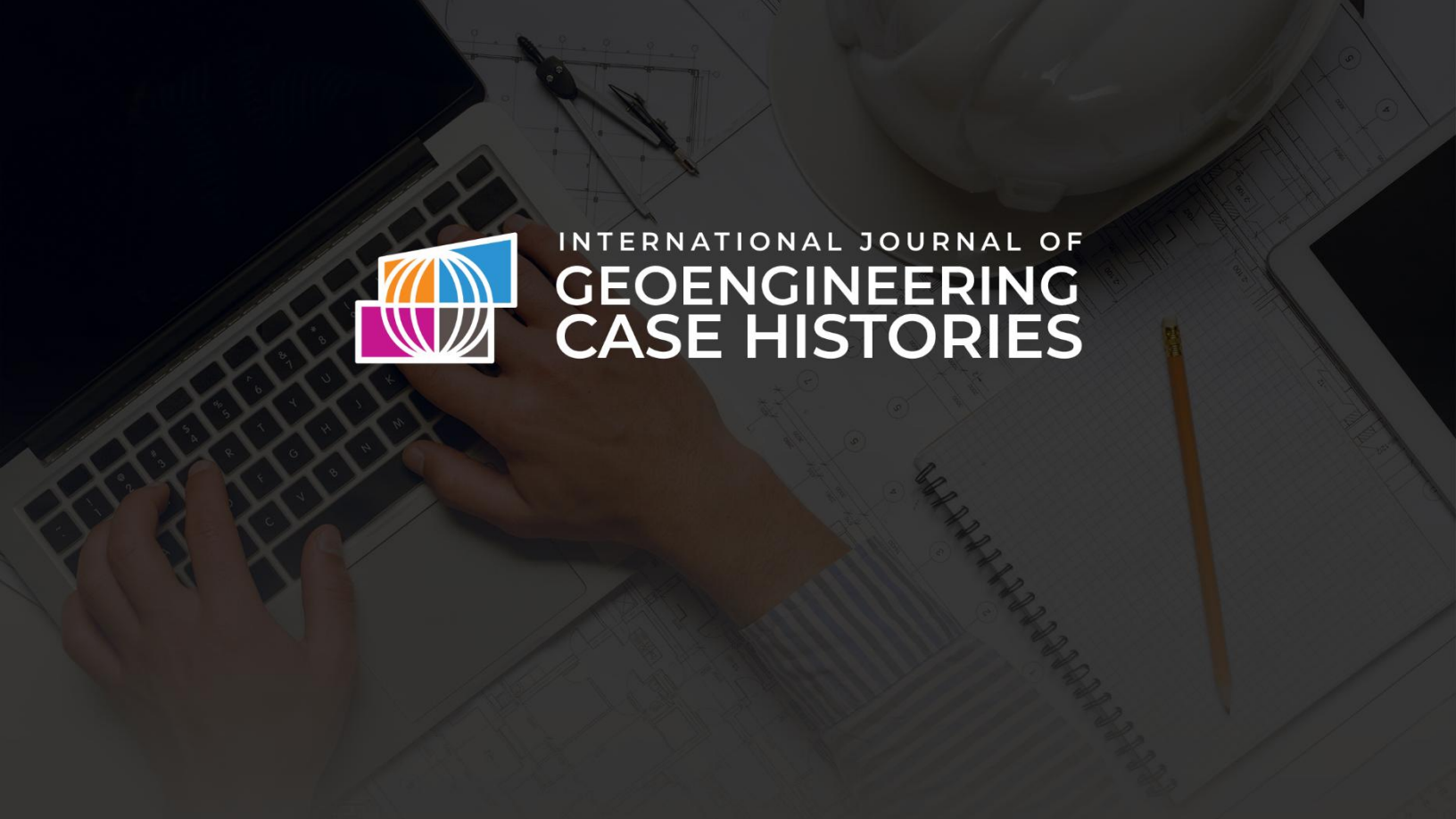

INTERNATIONAL JOURNAL OF
GEOENGINEERING
CASE HISTORIES

The Journal's Open Access Mission is generously supported by the following Organizations: